EMPIRICAL INDICATED LOSS ANALYSIS OF A SEMI-HERMETIC LIGHT-COMMERCIAL SPOOL COMPRESSOR

By

SETH J YARBOROUGH

Bachelor of Science in Mechanical Engineering
Oklahoma State University
Stillwater, OK
2018

Submitted to the Faculty of the
Graduate College of the
Oklahoma State University
in partial fulfillment of
the requirements for
the Degree of
Master of Science
May, 2021

EMPIRICAL INDICATED LOSS ANALYSIS OF A SEMI-HERMETIC

LIGHT-COMMERCIAL SPOOL COMPRESSOR

Thesis Approved:

Dr. Craig Bradshaw

Thesis Advisor

Dr. He Bai

Dr. Daniel Fisher

ACKNOWLEDGMENTS

First, I would like to thank my parents, family, and friends for all the love and support throughout the duration of my education, the patience and understanding shown for my hectic schedule has been an important key to a successful completion of this degree. Words can't describe how grateful I am for all of the unconditional love and support.

Second, I would like to thank Dr. Craig Bradshaw for inviting me to join the BETSRG research group. It's been a pleasure to have an advisor with so much constant enthusiasm, guidance, and positivity. He's always been willing make time for extra meetings and discussions. I've learned a great deal and I am thankful for this opportunity.

I am thankful to the CEAT employees, Gary Thacker, Dan Webb, and Aaron Bell for their willingness to help and provide support.

Thank you to everyone in the BETSRG research group. It's been a great pleasure to share this time with the students within the BETSRG research group. Everyone has always been supportive and happy to help one another. It's been a pleasure to spend so much time working with and around such a great group of people. I'm grateful for all the time shared taking trips and working together. A special thanks to Saad Saleem, Kalen Gabel, and Andrew Quinton. Thank you for all the memories.

I would also like to thank Jake Singleton for working alongside me for much of this project. He has always been so gracious with his time helping me with any and all of

Acknowledgments reflect the views of the author and are not endorsed by committee members or Oklahoma State University.

the unforeseen troubles that come with experimental work. It was a great privilege share an office for the better part of two years and to work alongside such a good friend.

Finally, I would like to thank Joe Orosz and Greg Kemp at Torad for sponsoring me and always taking care of me throughout this project. It's been a wonderful adventure to experience and learn from such a great group of characters. They were incredibly gracious with their time and energy, which allowed me to successfully complete this project and hopefully add some value to the work they're doing.

Acknowledgments reflect the views of the author and are not endorsed by committee members or Oklahoma State University.

Name: SETH J YARBOROUGH

Date of Degree: MAY, 2021

Title of Study: EMPIRICAL INDICATED LOSS ANALYSIS OF A SEMI-HERMETIC LIGHT-COMMERCIAL SPOOL COMPRESSOR

Major Field: MECHANICAL AND AEROSPACE ENGINEERING

Abstract: An analysis of the indicated losses is presented for a semi-hermetic, light-commercial, prototype, spool compressor. The spool compressor prototype was instrumented with five high-speed pressure sensors, three in the compression process, one in the discharge valve plenum, and one in the motor cavity. These sensors were triggered with a proximity sensor actuated by means of a custom rotary fixture attached to the compressor motor shaft. This coupling of rotational position and pressure measurements allowed the development of an indicator (pressure v. volume) diagram for the compression process. Additionally, the added sensor in the discharge valve plenum allowed for a de-coupling of discharge valve losses and flow losses within the discharge plenum itself. The sensor in the motor cavity allowed for an analysis of the flow losses leaving the compressor shell. The compressor was tested at five motor speeds (1100, 1300, 1500, 1700 rpm and line voltage) at condensing and evaporating temperatures ranging from 37.8 – 48.9 °C (90 – 130 °F) and -3.8 – 15.6 °C (30 -60 °F), respectively at a fixed suction superheat of 20 °R (11.1 K). Quantitative analysis shows that the suction and compression losses for this prototype compressor are relatively small compared with the discharge/valve losses. The total losses during the discharge process are generated by pressure drop and backflow through the discharge valve ports as well as when gas flows from the discharge plenum to out of the compressor body. It was found that a 5-6% compressor efficiency can be accomplished by redesigning the discharge plenum and motor cavity to reduce over pressurization. Further investigation into the valve dynamics need to be performed to improve the 11-12% loss in the valves. There is little dependence on operating condition for losses presented while the discharge losses tend to increase with and increasing speed and decreasing SDT. The work presented in this thesis is part of a broader initiative to improve the performance and functionality of the spool compressor specifically for low-GWP refrigerants.

TABLE OF CONTENTS

Chapter Page

LIST OF TABLES

LIST OF FIGURES

Figure Page

Figure Page

ABBREVIATIONS

BW	Boundary Work
CFD	Computational Fluid Dynamics
DAQ	Data Acquisition Equipment
DOE	US Department of Energy
DC	Discharge Cover/Discharge Plenum
DP	Discharge Pocket
EIA	US Energy Information Administration
GWP	Global Warming Potential
HVAC&R	Heating, Ventilation, Air Conditioning and Refrigeration
IVM	Ideal Mass Volumetric Efficiency
LV	Line Voltage
MC	Motor Cavity
PP	Process/Compression Pocket
RPM	Revolutions Per Minute
SP	Suction Pocket
SST	Saturated suction temperature
SDT	Saturated discharge temperature
TDC	Top Dead Center
US	United States

NOMENCLATURE

VARIABLES	UNITS	DESCRIPTION
$s_{\bar{x}}$	-	Random Uncertainty of Sample
s_x	-	Sample Standard Deviation
N	-	Sample Length
x_j	-	Measurement value
$\bar{x}$	-	Sample mean
P_{dis}	bar	Bulk system discharge pressure
$Comp_{leakage}$	-	Variable indicating amount of mass loss in compression
$P_{suction}$	bar	Bulk system suction pressure
V_{max}	cm^3	Max volume
V_{min}	cm^3	Minimum volume
$V_{dis,start}$	cm^3	Volume at the start of the discharge process
$L_{suction}$	$\mathrm{N-m}$	Suction losses
L_{comp}	$\mathrm{N-m}$	Compression losses
L_{valves}	$\mathrm{N-m}$	Valve losses
$L_{discharge}$	$\mathrm{N-m}$	Discharge losses
$L_{dis,plenum}$	$\mathrm{N-m}$	Plenum/cover losses
$L_{dis,MC}$	$\mathrm{N-m}$	Motor cavity losses

CHAPTER I

INTRODUCTION

As a result of changing efficiency standards for Heating, Ventilation, Air Conditioning and Refrigeration (HVAC&R) equipment, hydrofluorocarbon refrigerants such as R134a and R410A will be slowly phased out due to their high Global Warming Potential (GWP). Therefore, low GWP replacement refrigerants will start to replace them in the upcoming years. According to the US Energy Information Administration EIA (2011), and the DOE (2011) building data book, the consumption of electrical energy of HVAC&R systems in the residential and commercial sectors corresponds to 22%, and 18%, of all primary energy annually in the US, roughly 40% in total. Compressors are estimated to account for roughly 60% of that energy consumed in cooling and refrigeration systems Westphalen and Koszalinski (2001). As a result compressors in HVAC&R applications represent roughly 5% of total primary energy utilization in the US. Therefore, to ensure maximum efficiency of new HVAC&R systems it is critical to evaluate and analyze new HVAC&R equipment, especially compressors. Novel compressors are especially critical to evaluate in great detail to ensure adoption of new technology that creates a meaningful increase in system efficiency.

Various methods over time have been used to evaluate the performance of compressors. Broadly, bulk compressor testing is accomplished by testing a compressor at set conditions for suction, discharge, speed, and superheat among others. Once the compressor reaches steady state at the desired set conditions the test setup data is saved and used to evaluate the compressor bulk conditions such as isentropic and volumetric efficiencies. The isentropic and volumetric efficiencies among other parameters are often used to evaluate bulk compressor performance. The room for improvement for those parameters is becoming more and more challenging to identify as the efficiencies increase. A macro-analysis with those parameters is performed in Orosz et al. (2012, 2014) by comparing the bulk efficiency metrics with those of other existing compressor technologies. Additional macro-analysis and bulk testing was performed following this work using R134a and R1234ze to further contribute to the overall goal of improving the spool compressor. The additional bulk testing performed on the spool compressor is described in Appendix D. While those bulk parameters can still be useful for macro-analysis of compressor performance there is often a need for a more detailed breakdown and analysis of losses within a compressor. This work primarily focuses on the detailed loss analysis specifically on the 8$^{\text{th}}$ generation spool compressor. The following sections cover the ideas and techniques used in this work to perform a more detailed breakdown of the losses within a compressor by means of an indicator diagram.

1.1 General Compressor Description

For the readers that are unfamiliar with what a compressor is, and what a compressor is used for, this section will give a brief overview to help provide context for the analysis presented. There are two different general categories of compressors, positive displacement and dynamic, but for this purpose only positive displacement compressors will discussed.

A compressor takes a volume of a fluid at it's inlet and compresses it to decrease the volume of the fluid as it moves the fluid to the outlet. By reducing the volume of the fluid, whether it be air or refrigerant, it increases the pressure of the fluid. In the case of an air compressor the compressor forces the air into a storage cylinder and continues to increase pressure until the cylinder reaches a desired set pressure. In the case of the compressor analyzed in this work the compressor acts as the driving force in the refrigeration cycle.

1.2 Literature Review

1.2.1 Compressors Performance Analysis

In order to understand how compressor performance can be improved it's important to understand what elements make up the the losses that take away from the performance. The elements that make up the electrical input power loss into the compressor can be defined as the sum of the motor loss, mechanical loss, and indicated loss. Each of these losses play a meaningful role in improving the overall efficiency of a compressor. The primary loss evaluated in this work is specifically the indicated loss present in the working process of the spool compressor.

Jacobs (1976) presented an overview of analytic and experimental methods to serve as a guide to identify the performance losses of a reciprocating hermetic compressor. The indicator diagram is one of the methods shown that can be utilized to quantify compression, suction, and discharge losses, which are denoted indicated losses. In an example presented by Jacobs (1976) it was shown that the modification of the valve ports reduced the cylinder over pressurization, therefore reducing the indicated loss and improving the performance of the compressor. These methods used for the indicator diagram were implemented in further detail by Rigola et al. (2002), Real and Pereira (2010), Huang et al. (2018), and Bauer (1988) on reciprocating compressors with similarly useful results. Rigola et al. (2002) was able to effectively compare the indicated work experimental data with numerical data utilizing the indicator diagram which resulted in the verification of a numerical model that allowed for a suggestion for flow area estimation improvement within that model. Real and Pereira (2010) used a similar method to gain insight on the valve function for the evaluation of back flow. Huang et al. (2018) utilized the indicator diagram to analyze the work loss done while analyzing the opening and closing delay times of the valves to suggest an improved valve plate design. Bauer (1988) specifically investigated the reciprocating compressor valve loss pockets showing on the indicator diagram that the losses in the suction can be attributed to both the valves and flow restrictions within the valve chambers. Bauer (1988) concluded that the optimizing the flow area around the valves is more economical and requires less complex valve designs to impact the losses. The successful utilization of the indicator diagram in these works have shown that the indicator diagram method of performance analysis can be useful in the improvement of reciprocating compressors.

The methods implemented in the indicator diagram can also be applied to other types of positive-displacement compressors. Haugland (1990), Stošic et al. (1992), and Peng et al. (2002) each investigated an experimental performance analysis by means of indicator diagrams on screw compressors. Haugland (1990) developed a twin screw compressor model and utilized the indicator diagrams as a mechanism to experimentally validate the gain understanding of the model. Stošic et al. (1992) analyzed the influence of oil injection on the screw compressor. Nikolov and Brümmer (2016) investigated indicator diagrams for water injected screw expander. Nomura et al. (1984) performed a loss analysis on a rotary compressor before and after making changes that improved that compressors performance by approximately 12%. Bianchi and Cipollone (2015); Yang et al. (2009); Huang and Yang (2008) also all present work on sliding vane compressors showing similar methods and reasoning to sensor placement in vane compressors. The previous vane compressor work is useful to see how and where others measured and instrumented other vane compressors with a similar function. The vane compressors work was heavily focused on mechanical efficiencies and friction while this work is focus on indicated losses. The additional fidelity provided by the indicated loss analysis includes significantly more information than isentropic and volumetric efficiencies do. As a result, indicator diagrams have been utilized for many different positive displacement compressor types to both quantify compressor loss and to validate compressor models. This study will apply this technique to a novel compression technology, the spool compressor, to examine opportunities for improving a semi-hermetic commercial air-conditioning prototype.

1.2.2 Spool Compressor Background and Motivation

The rotating spool compressor is a novel positive displacement rotary machine. The rotary spool compressor mechanism operates using the same compression mechanism as a sliding vane compressor, but addresses some of the problems that sliding vane compressors experience. The primary problems and differences address are described by Kemp et al. (2008) who first introduced the compressor by experimentally testing the feasibility and proof of concept using air. Kemp et al. (2008) was able to show that in the early design state the rotary spool compressor could perform comparatively with other existing technologies. The challenge with the solutions offered by other technologies, addressing the problems of the traditional vane compressor, is with the associated cost in manufacturing complex machines. The spool compressor, however, offers a unique economical design that requires less cost in the manufacturing process.

The spool compressor has since undergone a meaningful progression in development as several prototype generations have been developed and tested. The spool compressor has been developed for various applications in the HVAC&R industry. The improvement from each prototype generation has presented additional opportunity for insight into the best design optimization and application. Each prototype has explored different aspects of the compressors specific intricacies that have been integrated into the design.

In 2012 several different works were presented on the spool compressor technologies. Orosz et al. (2012) presented the results of the performance characteristics of four prototype spool compressors using R410A and R134a comparing the performance efficiencies with the other compressor technologies. The study showed that the compressor tested still needed further evaluation to be more competitive with existing technologies.

Next, Bradshaw and Groll (2013) developed a comprehensive simulation model of the spool compressor that consisted of of several sub-models including geometry, friction, leakage, and heat transfer. The model was experimentally validated using a R410A machine. The results of the model validation showed that there was some aspects that were predicted reasonably well and others that needed further sub-model development. This led to the further development of the sub-models to improve sealing elements of the as presented in Bradshaw (2013) and Bradshaw et al. (2016). Further investigation was needed generate a more complete understating of the individual processes within the compressor.

Bradshaw et al. (2016) presents a loss analysis on the 5$^{\text{th}}$ generation spool compressor prototype using similar methods to develop an indicator diagram based on dynamic pressure measurements. The indicator diagram enabled the evaluation of the indicated losses of the 5$^{\text{th}}$ generation spool compressor. The loss analysis resulted in the understanding that the spool seals and the discharge valves were primary cause of excessive leakage and friction. Additionally, the discharge valves were identified in this analysis as one of the largest indicated losses. As a result, further development and optimization the valve system was performed and modeled in Wood et al. (2016).

The development of the design and understanding of the process gained from this from the previous work led to significant efficiency improvement from the 5$^{\text{th}}$ to the 6$^{\text{th}}$ generation of spool compressor as presented in Orosz et al. (2014). Orosz et al. (2014) presented the results from the improved 6$^{\text{th}}$ generation spool compressor. This R410A, 5-ton displacement, prototype spool compressor performance efficiencies were compared again with the similar sized current market compressor technologies. The comparison showed that the 6$^{\text{th}}$ generation prototype performance was competitive in the current market in the 5-ton range. The improvement shown indicates the benefit of the utilization of the various tool and knowledge gained from the previous generation testing and modeling. The 7th generation, R134a, 40-ton, prototype spool compressor presented initial performance data in Orosz et al. (2016). This R134a, 40-ton displacement, prototype designed using information from the model developed by Bradshaw et al. (2016). The new R134a prototype performed well across a large range of test conditions showing promise and room to improve efficiency.

Bradshaw et al. (2018) explored the potential for efficiency improvement by performing an indicated loss analysis on the 7th generation of prototype spool compressor, a 40-ton R134a prototype machine. The results of this study presented the two largest areas of opportunity to increase the efficiency to be in the discharge plenum and discharge valves. A redesign of the discharge plenum was recommended for a potential 4-5% improvement in efficiency. The results suggest that the largest opportunity for improvement in this prototype is a re-design of the discharge plenum. The success of an indicated loss analysis on the 7th generation spool compressor prompted interest in exploring the potential improvement of the 8th and current generation of the prototype spool compressor, shown in Figure 2.1. This study will present the experimental methodology, data analysis techniques, and indicated loss analysis results and suggest changes to the 8th generation prototype to maximize its efficiency.

1.3 Project Overview

This project focuses on utilizing a combination of the methods described in works presented in section 1.2 to perform a micro-analysis of the 8th generation, 30-Ton, novel rotary spool compressor by means of an indicated loss analysis. This analysis the first indicated loss analysis on the 8th generation spool compressor. The primary objective of this project was to instrument, test, and evaluate the losses within the working process to further gain insight that adds to furthering the development of the next generation spool compressor. This project is a part of the broader objective of the development of the spool compressor for new low-GWP refrigerants. The data collected in this analysis in addition to the testing discussed in Appendix D will aide in further model development and compressor design.

CHAPTER II

EXPERIMENTAL METHODOLOGY

To generate an indicated loss analysis it is first necessary to measure dynamic pressure data and compressor shaft position, which can be analyzed into the relevant indicated losses. This chapter will focus on the methodology of the collection of data required to generate an indicator diagram. The general method to create an indicator diagram is to simultaneously measure both instantaneous dynamic chamber pressure and angular position of the motor shaft of a positive displacement compressor. This is traditionally done by mounting multiple pressure transducers into the working chamber to measure the pressure dynamically and instantaneously at the suction, discharge, and compression of the compressor as done by Haugland (1990) with a twin-screw compressor. The pressure measurement locations vary depending on the specific compressor so that the entire process is captured with the combination of sensors, often times having part of each process overlapping with another sensor. Generally, either piezoelectric or piezoresistive pressure transducers are used because they can measure dynamic pressure at a high sampling rate.

In order to couple pressure and volume the rotation angle needs to be captured in some fashion, typically this has been done using a rotary encoder to measure shaft position. Rotation angle at any given instant is then used to calculate the volume of the suction, discharge and compression chamber allowing for the coupling of the pressure and volume. Pressure and volume then are aligned and make up the indicator diagram. Rigola et al. (2002) and Huang et al. (2018) used similar methods to produce indicated diagrams of reciprocating compressors. This is a process that follows closely with the work presented in Bradshaw et al. (2018) on a 7^{th} generation open drive spool compressor and this work continues from that effort.

The indicated loss analysis of the 8^{th} generation spool compressor will follow a similar methodology. The following section describes the installation and setup of the experiment to collect the test data that creates an indicated loss analysis on the 8^{th} generation spool compressor. This includes the sensor selection, placement, and calibration as well as an uncertainty analysis and the final test matrix of operating conditions that are collected and analyzed.

2.1 Sensor selection, location, calibration, and procedure

A 30-ton, semi-hermetic, prototype spool compressor is fitted with three Meggitt 8530B-500 high-speed piezoresistive pressure sensors. These pressure transducers are used because they are able to measure static and dynamic pressure, and they have a resonant frequency of 1,000,000 kHz with a maximum pressure range up to 34.47 bar. Therefore, the transducers have no trouble sampling dynamic pressures in this analysis. The sensors are placed at locations which will allow for easy installation of the sensors and for most of the process pressures to be measured at all rotor angles, called SP, PP, and DP, respectively. Furthermore, an additional two sensors were placed downstream of the discharge valve assemblies but upstream of the discharge manifold plumbing connection of the test stand, called DC and MC, respectively. Figure 2.1 and Figure 2.2 shows the physical locations of these sensors relative to the suction and discharge of the compressor. The angular locations of the three sensors in the process section are shown in Figure 2.3, which is an axial view schematic of the compressor cylinder with the sensor angles relative to Top-Dead-Center (TDC).

The placement of the first sensor, SP, is at 90 degrees from TDC, just past the suction port, so that each time the vane crosses the suction port the SP sensor can capture a large majority of the suction chamber. The second sensor, PP, is placed

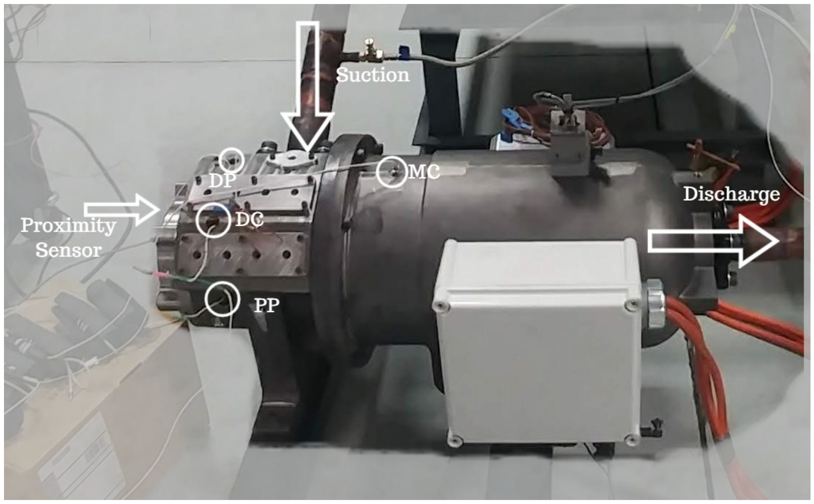

Figure 2.1: 8th generation, R134a, 30-ton, semi-hermetic, spool compressor prototype with high-speed pressure sensors installed showing motor cavity (MC) sensor, compression chamber (PP) sensor, discharge (DP) and discharge plenum (DC). Suction (SP) sensor not in view.

at 249 degrees from TDC as close to the discharge valves as possible in an attempt to capture all of the compression process with a single sensor for all of the test conditions. The third sensor, DP, is placed at 343 degrees past TDC at the end of the discharge process to capture the majority of the discharge process. The DP sensor is additionally recessed from the compressor cylinder approximately 10 mm in an attempt to reduce any potential pressure fluctuations. The placement of the three sensors allowed for the suction, compression and discharge processes to be capture with each of the respective sensors. Figure 2.4 shows the volumes of the suction, discharge, and compression as a function of crank angle with the placement of the three primary pressure transducers overlaid. The final two sensors, DC and MC are placed in the discharge valve plenum and motor cavity in convenient locations that allow for easy installation while still capturing the pressure data from those regions. The gas flow through the valves, discharge plenum, motor cavity and flow over the motor leaving the compressor is shown in Figure 2.5. The only regions which cannot be measured are near the TDC area of the compression process on both the suction and discharge side of the compressor. Since the volume in this region is small in

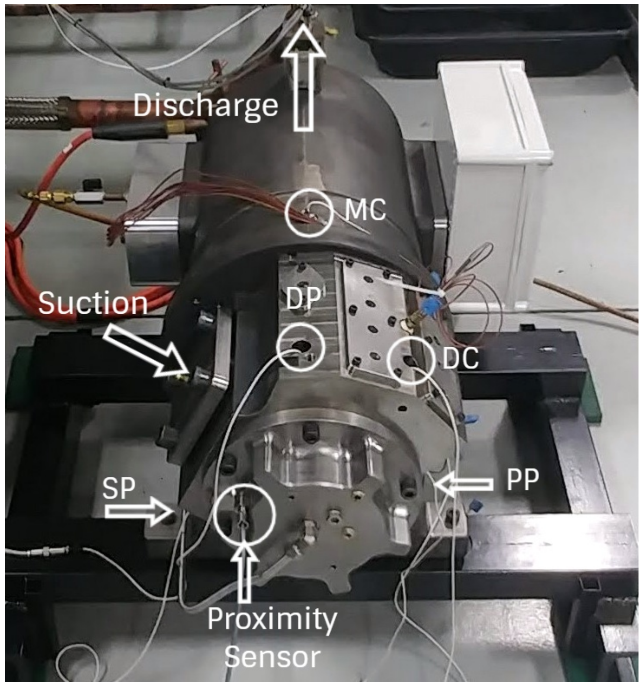

Figure 2.2: 8th generation, R134a, 30-ton, semi-hermetic, spool compressor prototype with high-speed pressure sensors installed showing motor cavity (MC) sensor, compression chamber (PP) sensor, discharge (DP) and discharge plenum (DC). Suction (SP) sensor not shown because it's not in view.

comparison to the other volumes it is assumed that any losses that is unable to be measured is also small, therefore that loss in considered negligible.

The piezoresistive pressure transducers used in this analysis are used in conjunction with two bridge amplifiers (Endevco Model 126) to supply the transducers with power, reduce noise, and amplify the output signal into a signal that can be accurately read with Data Acquisition Equipment (DAQ). These piezoresistive pressure transducers used can be susceptible to a change in the zero measured output as a result of electrical installation (i.e. cable length and conductor quality) and mechanical installation (i.e. applied torque and wire strain). To mitigate the influence of error due to mechanical installation each of the five sensors was carefully installed with the recommended 1.69 N-m of torque and the strain on the sensors were minimized. To reduce influence as a result of electrical installation each sensor was electrically insulated at each of the connection points and were wired to ground at the signal con-

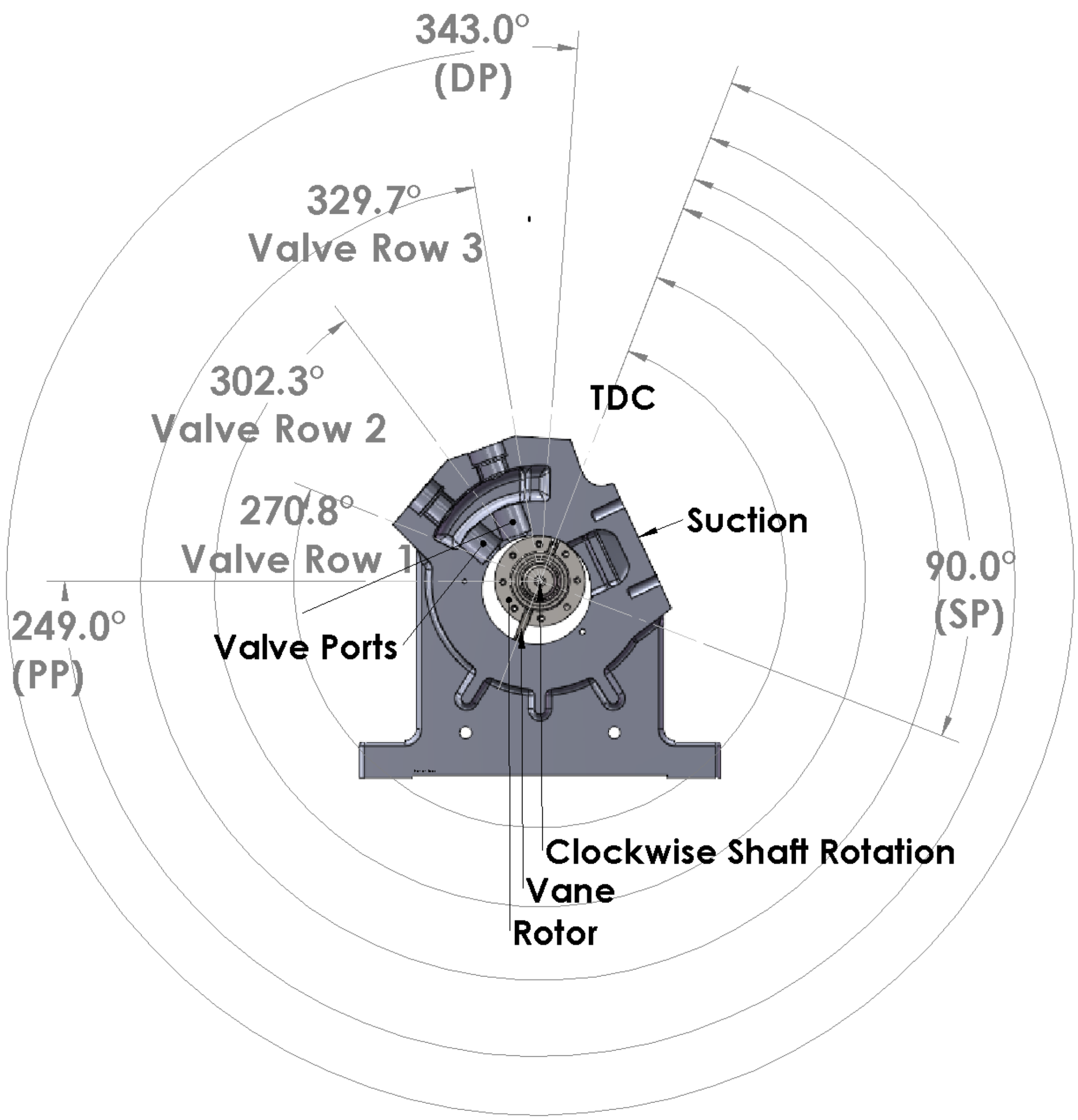

Figure 2.3: Axial view of compressor cylinder block highlighting the angular location of in-pocket sensors and valve location relative to vertical and the compressor top-dead-center (TDC).

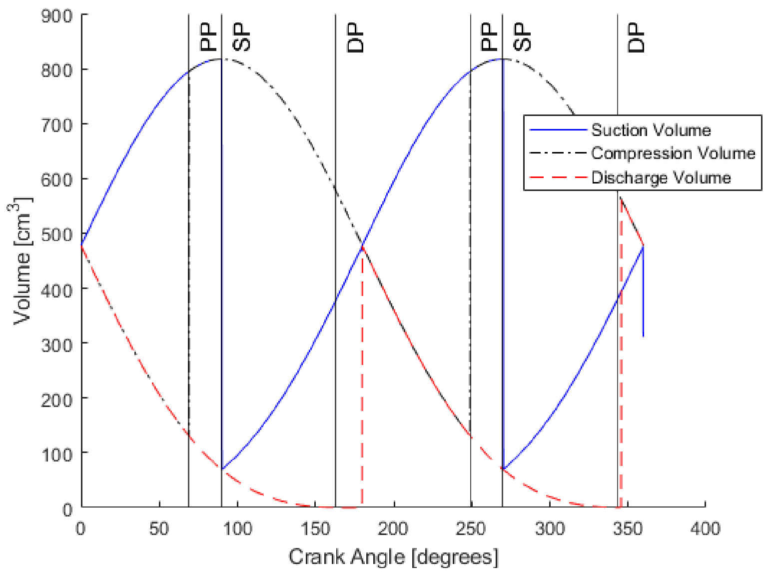

Figure 2.4: 8th generation, R134a, 30-ton, semi-hermetic, spool compressor Volume vs. Crank angle curve showing the sensor locations.

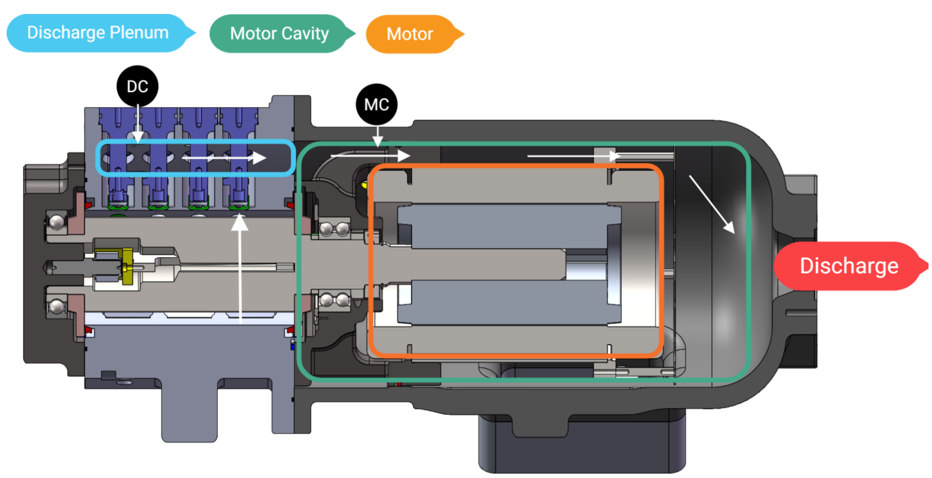

Figure 2.5: 8th generation, R134a, 30-ton, semi-hermetic, spool compressor cutaway showing the flow path through the valves, discharge plenum, motor cavity, and into the discharge.

ditioner. Each sensor was also calibrated in-place using dry nitrogen and a pressure reference measured using a Druck [DPI 612] with an accuracy of 0.0086 bar before each set of tests. The calibration was additionally repeated at the end of each set of tests to verify no significant changes to the calibration occurred.

The design of semi-hermetic 8^{th} generation compressor didn't allow for a rotary encoder to be easily implemented. To measure shaft speed and position an inductive proximity sensor (Sensor Solutions S50FW-18ADSO-ODSB5) is used instead. Figure 2.6 shows the axial view of the physical location of the proximity sensor relative to the suction of the compressor. The proximity sensor is used in conjunction with a custom rotary fixture affixed to the rotating spool such that the proximity sensor triggered when the vane of the compressor was at compressor Top Dead Center (TDC). This was used as a datum, or index, and all angles were measured in reference to this location. From the trigger, time is measured using the Data Acquisition Equipment (DAQ) and the shaft speed is assumed to be constant within one rotation. This assumption is further explored in greater detail in Chapter III and is found to be reasonable. Using the measured time and the aforementioned assumption regarding speed allowed for an inference of the shaft position at any instant in the rotation.

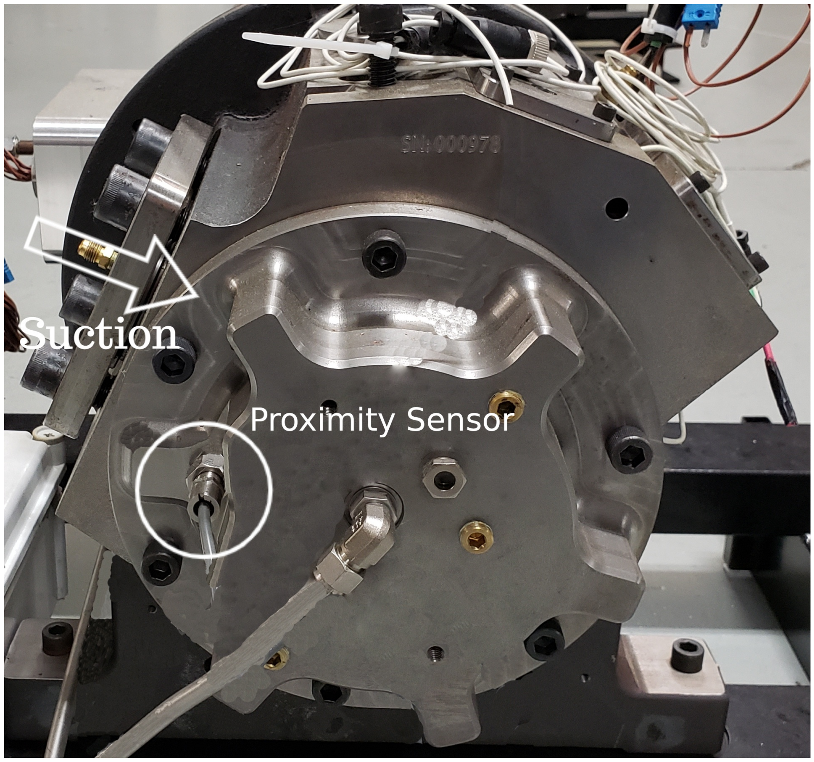

Figure 2.6: Axial view of 8^{th} generation, R134a, 30-ton, semi-hermetic, spool compressor prototype showing proximity sensor location.

2.2 Experimental procedure and test conditions

The compressor is first operated until it reaches steady-state conditions at a prescribed operating condition using the hot-gas bypass load stand environment described in Orosz et al. (2016). Figure 2.7 shows the overall test setup for spool compressor and the general locations of the primary sensors used in this thesis. The high speed pressure measurements, proximity sensor, speed, electrical work and the bulk suction pressure and temperature are shown. The hot-gas bypass load stand is operating and collecting steady-state data using it's own independent DAQ setup. An additional separate DAQ environment, implemented in LabVIEW (2013), shown in Figure 2.8 was developed and controlled to calibrate and collect the pressure transducer and proximity sensor data. The primary function of this DAQ setup was to provide an act as an addition to load stand environment in order to read, calibrate, and collect the high speed pressure data that allowed for the development of the indicator diagram.

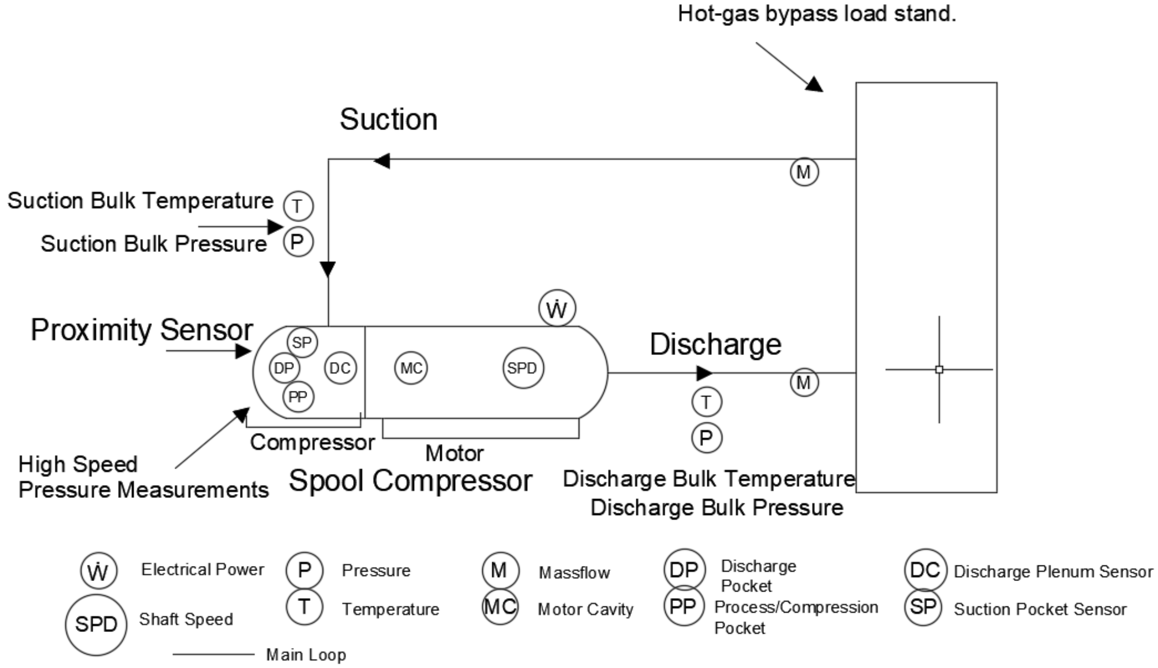

Figure 2.7: Schematic of the overall test setup showing the connection to the hot gas bypass load stand and the primary sensor locations for the both the load stand and spool compressor.

Figure 2.8: Data Acquisition (DAQ) front panel view used to collect indicated loss data.

The pressure sensors are sampled at 70,000 samples per second, triggered using the inductive proximity sensor to start sampling at TDC, and sampled for a length of time that ensures at least one complete rotation of the shaft. The sampling length of time was set by selecting the number of samples desired, for most conditions 4600 samples were taken in order to capture a minimum of one complete rotation. This process was repeated 20 times per operating condition and these samples were averaged into a single sample which reflects the behavior at the current condition.

The prototype compressor was operated using refrigerant R134a at five shaft speeds, various Saturated Discharge Temperatures (SDT) and Saturated Suction Temperatures (SST) at a fixed compressor inlet superheat of 20 °R for a total of 36 data points. Various speeds were explored for several conditions in the test matrix to get an indication of what variables were affected by different speeds and if they had followed any noticeable trend. SST, SDT, and superheat were all swept in the test matrix to capture a wide range of test conditions that, based on previous spool compressor indicated loss testing, were found to be useful when looking for trends. The final test matrix collected for this study is presented in Table 2.1. The limited SST range for certain speeds and SDT are constrained by the limits of the test environment described in Orosz et al. (2016). Test condition 8, bolded and underlined in Table 2.1, is used as the illustrative example, throughout this work as it represents the typical behavior of the compressor.

Table 2.1: Final test matrix of 36 operating conditions (presented with various saturated suction and discharge temperatures, SST and SDT, respectively) with a fixed 20 °R superheat and shaft speeds.

<table>
<tr><th>Speed</th><th>SST</th><th>Test #</th><th>SDT</th><th>Speed</th><th>SST</th><th>Test #</th><th>SDT</th></tr>
<tr><td>rpm</td><td>°C</td><td>-</td><td>°C</td><td>rpm</td><td>°C</td><td>-</td><td>°C</td></tr>
<tr><td rowspan="4">1100</td><td rowspan="4">4.44</td><td>5</td><td>37.78</td><td rowspan="4">1300</td><td rowspan="4">4.44</td><td>6</td><td>37.78</td></tr>
<tr><td>4</td><td>43.33</td><td>3</td><td>43.33</td></tr>
<tr><td>11</td><td>48.89</td><td>10</td><td>48.89</td></tr>
<tr><td>12</td><td>54.44</td><td>13</td><td>54.44</td></tr>
<tr><td rowspan="4">1500</td><td rowspan="4">4.44</td><td>7</td><td>37.78</td><td rowspan="10">1700</td><td>1.67</td><td>34</td><td>48.89</td></tr>
<tr><td>2</td><td>43.33</td><td rowspan="6">4.44</td><td>8</td><td>37.78</td></tr>
<tr><td>9</td><td>48.89</td><td>1</td><td>43.33</td></tr>
<tr><td>14</td><td>54.44</td><td>16</td><td>48.89</td></tr>
<tr><td rowspan="14">LV</td><td rowspan="4">-1.11</td><td>17</td><td>37.78</td><td>15</td><td>54.44</td></tr>
<tr><td>18</td><td>43.33</td><td>32</td><td>32.22</td></tr>
<tr><td>19</td><td>48.89</td><td>31</td><td>35.00</td></tr>
<tr><td>20</td><td>54.44</td><td>33</td><td>48.89</td></tr>
<tr><td rowspan="4">4.44</td><td>30</td><td>37.78</td><td>7.22</td><td>35</td><td>48.89</td></tr>
<tr><td>27</td><td>43.33</td><td>12.78</td><td>36</td><td>48.89</td></tr>
<tr><td>26</td><td>48.89</td><td colspan="4" rowspan="8"></td></tr>
<tr><td>21</td><td>54.44</td></tr>
<tr><td rowspan="4">10</td><td>29</td><td>37.78</td></tr>
<tr><td>28</td><td>43.33</td></tr>
<tr><td>25</td><td>48.89</td></tr>
<tr><td>22</td><td>54.44</td></tr>
<tr><td rowspan="2">15.56</td><td>24</td><td>48.89</td></tr>
<tr><td>23</td><td>54.44</td></tr>
</table>

CHAPTER III

DATA UNCERTAINTY, REDUCTION, AND ANALYSIS

This section will present the procedures used to reduce the collected data, estimate the uncertainty associated with the calculated losses, and calculate the suction, compression, and discharge indicated losses within the compressor. Additionally, two external indicated losses, the plenum and motor cavity losses are also estimated as shown in this section.

3.1 Uncertainty and Data Reduction

The uncertainty of the loss measurements is represented as a total relative uncertainty of the boundary work, as shown in the section below, this includes contributions from the high-speed pressure measurements and the volume calculation.

3.1.1 Uncertainty and Data Reduction of Pressure Measurement

High speed pressure data was taken as described in Chapter 2.2 where 20 repeated samples of pressure data was taken for each condition. That pressure data was first evaluated by reading in all the raw pressure data for each of the five sensors and converting those pressures to absolute pressure by adding the ambient pressure. Those pressures were then overlaid on top of each other for every one of the 20 samples and plotted as a function of crank angle as shown in Figure 3.1a for test condition 8. Overlaying all the pressure samples taken allowed for a verification that the proximity sensor trigger mechanism triggered at the correct location each time the sample was taken. The appropriate gap between the proximity sensor and the custom rotary fixture that triggered the data collection for each point was initially difficult to judge. Therefore, resulting in samples being triggered incorrectly as shown in Figure 3.2. The overlaying of the 20 samples proved to be useful for identifying the appropriate gap that produced correct triggering. Those 20 samples, as mentioned previously, were then averaged into a single sample that reflects the behavior of the current condition as shown by Figure 3.1b. Figure 3.1 shows that the 20 sample points come rather close to one another and follow a similar trend indicating that the pressures measured were consistent with one another,resulting in a clean pressure sample to be further evaluated.

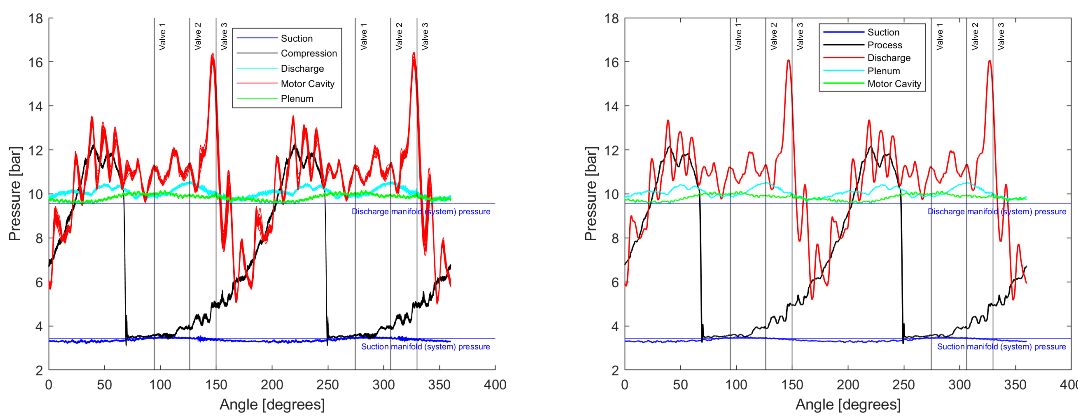

(a) All 20 pressures of each sensor overlaid.

(b) Average resulting pressure signals.

Figure 3.1: The five final pressures as a function of crank angle overlaid with the valve positions.

The total uncertainty of the pressure measurement is calculated as a quadrature addition of the random and systematic uncertainty. The systematic uncertainty of the pressure sensors is 0.172 bar, as verified by calibration, and is assumed to be fixed. The random uncertainty in the pressure measurement is calculated using methods described in ASME-PTC-19.1 (2013) with the 20 sample points taken per operating condition and calculated throughout the rotation of the shaft using Equation 3.1.

$$s_{\bar{x}} = \frac{s_x}{\sqrt{N}} \tag{3.1}$$

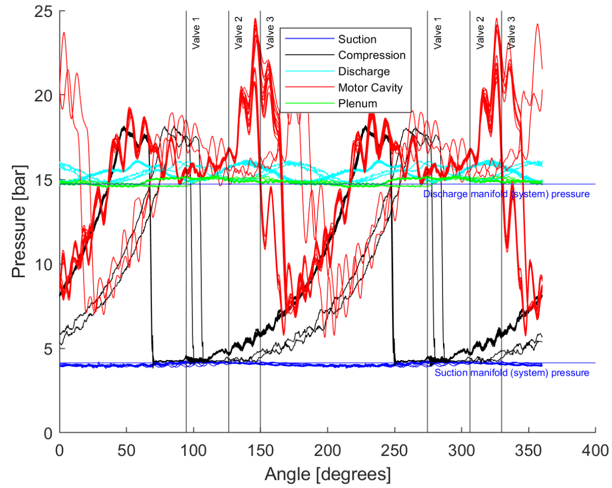

Figure 3.2: All 20 pressures of each sensor overlaid showing off triggered samples.

where s_x is the sample standard deviation over the sample length, N (20 points), given by Equation 3.2, in which x_j is the measurement value and $\bar{x}$ is the sample mean.

$$s_x = \sqrt{\sum_{j=1}^{N} \frac{(x_j - \bar{x})^2}{N-1}} \tag{3.2}$$

The pressure measurement consists of 70,000 samples per second and each of those samples were taken 20 times, therefore the random uncertainty is calculated for each of the samples. Then, using the random and systematic uncertainty, a total uncertainty was found for each of the pressure sensors. Next, The RMS (Root Mean Squared) for all of the total uncertainties for each of the sensors was taken. The RMS for each of the sensors was then averaged and used as the effective value representing the total uncertainty of the pressure measurements. That calculated total uncertainty of the pressure measurement ranged from 0.172 bar to 0.405 bar depending on the sensor and operating point. The largest uncertainty consistently came from the discharge pressure sensor (DP). Test condition 8, from Table 2.1, has a total uncertainty of the pressure ranging from 0.172 bar to 0.177 bar having a relatively small random uncertainty.

3.1.2 Uncertainty associated with fixed compressor speed assumption on the volume calculation

The volume calculation is less straightforward than reducing the pressure down to the final sample. In order to find the volume of the compressor it was first necessary to find the crank angle of the process. Since a rotary encoder wasn't able to be used for this testing the crank angle was found by multiplying an assumed fixed compressor speed and the time measured with the DAQ during testing. This is possible because the inductive proximity sensor installed on the compressor triggers once every rotation at TDC, which gives a clear start point for the DAQ measured time. The resulting crank angle and fixed speed were then used with the geometric model presented in Bradshaw and Groll (2013) to produce the volume in the compressor suction, compression, and discharge pockets at each crank angle. The output volume from the model is then used to assign the appropriate volume at each crank angle for each of the sensors. This is accomplished using the angular location of each sensor and evaluating which of the three pocket volumes is exposed to the sensor at each crank angle. The volumes for each sensor are then used to produce and evaluate the indicator diagram.

The assumption used in this work is that the rotational speed of the compressor remains constant throughout a single rotation. However, as mentioned in Huang and Yang (2008) the downside to not using a rotary encoder is that there are changes in shaft torque throughout the compression process that necessitate that the shaft speed is not strictly uniform throughout a single rotation. To quantify the uncertainty of the effect this assumption has on the volume calculation an analysis was performed using high-fidelity shaft position information collected from a similar spool compressor prototype, using an unpublished dataset collected during experiments presented in Bradshaw et al. (2018). Bradshaw et al. (2018) collected data on an open-drive spool compressor prototype, with similar geometric characteristics and operating parameters as the compressor in this work. Bradshaw et al. (2018) measured shaft

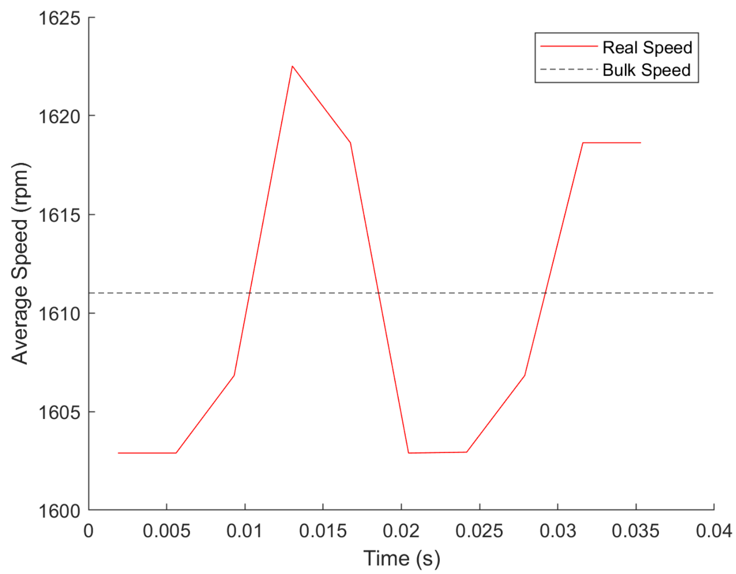

Figure 3.3: Encoder-measured speed variation over time for the open-drive, R134a, prototype spool compressor presented in Bradshaw et al. (2018).

position using a rotary encoder with 4096 steps/revolution that was also tested with R134a. Using the position data from the rotary encoder it is possible to estimate the variation in shaft speed over a rotation. For an operating condition most similar to test condition 14 in this study, it was found that the shaft speed in the open-drive prototype varied by no more than 20 rpm as shown in Figure 3.3.

The resulting differences in instantaneous volume calculated using fixed speed and the encoder speed was then estimated using the geometric model presented in Bradshaw and Groll (2013). It was found that the assumption of fixed speed would result in errors in volume averaging 0.67%. An additional assumption is then made that the open-drive and semi-hermetic mechanism operation is similar enough that the uncertainty in the both compressors volume calculations will be roughly the same. The following paragraphs will present the analysis used to conclude the fixed speed assumption is sufficient for this analysis.

3.1.2.1 Fixed Speed Assumption Evaluation

The calculation of the volume using the geometric model presented in Bradshaw (2013) requires detailed information about the compressor geometry and angular shaft position. Since the angular shaft position calculation relies upon the compressor speed the evaluation of the fixed speed assumption is done by comparing the volume calculated using the angular position of the encoder as the baseline and comparing it with the volume calculated using the fixed speed assumption.

To get an idea of how much the speed varied during each rotation it was first necessary to select data from Bradshaw et al. (2018) that was similar to the test conditions presented in 2.1. The data selected was most similar to test condition 14 and the data contained torque and rotation angle. The angular location from the encoder was used to calculate volume and is referred to as the encoder volume. Knowing the sample rate, angle, torque, and trigger location for the data allowed for the speed at each sample point to be inferred. This speed calculated is referred to as the real or instantaneous speed. However, due to the sample rate being very high, the speed needed to be averaged over an interval that encompassed approximately 250 samples throughout the rotation. The result, shown in Figure 3.4, shows the torque, averaged speed over each internal, and the bulk speed with respect to time. The averaged speed over each interval represents the real or instantaneous speed we expect to be happening with the change of torque. The bulk speed measured from the test load stand is then used for the fixed speed assumption.

In order to compare the effects of the real speed and fixed speed the volume for the suction, discharge, and compression were each found using the angular position of the encoder and the angular position found using the fixed speed. The angular position data from the encoder is believed to produce the most accurate volumes since it doesn't rely on speed to find the angular position, therefore, it is used as the baseline of comparison. The total volumes of the suction, discharge, and compression

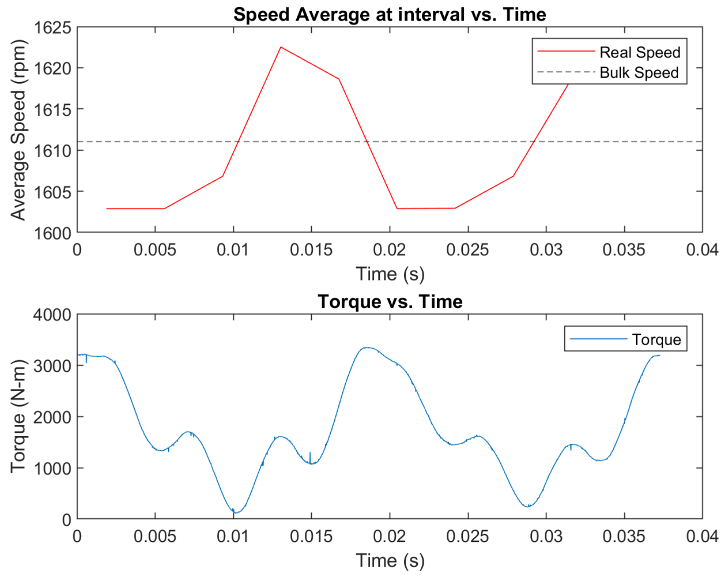

Figure 3.4: Encoder-measured speed, fixed speed and Torque over time for the open-drive, R134a, prototype spool compressor for an unpublished dataset collect during the experiments presented in Bradshaw et al. (2018).

are combined and compared for the encoder volume and the fixed speed volume as shown in Figure 3.5.

Figure 3.5 shows the volume curve for each of the both methods used to calculate the volume, respectively, fixed speed, and encoder angular position. The difference in volume calculated by the encoder position and fixed speed is calculated for the suction, discharge, and compression. The resulting differences in volume for the suction, discharge and compression are then averaged to find a resulting mean average error of 0.67% taken for the entire volume calculation as shown in Figure 3.6. The small error as a result of fixed speed indicates that the fixed speed assumption is a reasonable.

The primary purpose of this exercise was to evaluate the effects of the fixed speed assumption. That consisted of using data from and similar machine that allowed for a more accurate representation of angular location of the shaft by means of a rotary encoder then applying the fixed speed assumption method from this work to that of the different machine to make a baseline comparison to produce a rough uncertainty

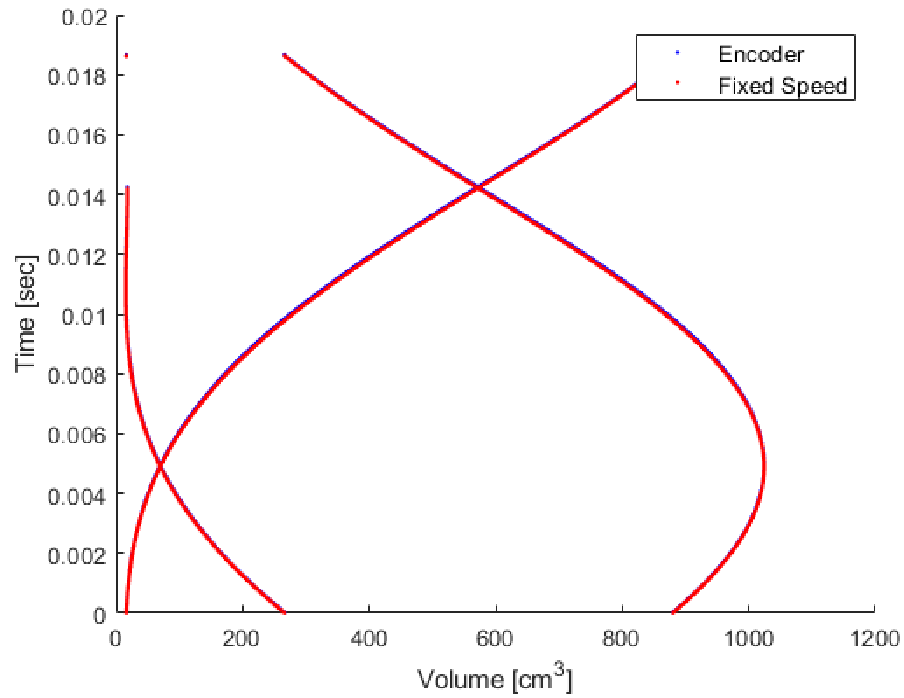

(a) Entire volume comparison.

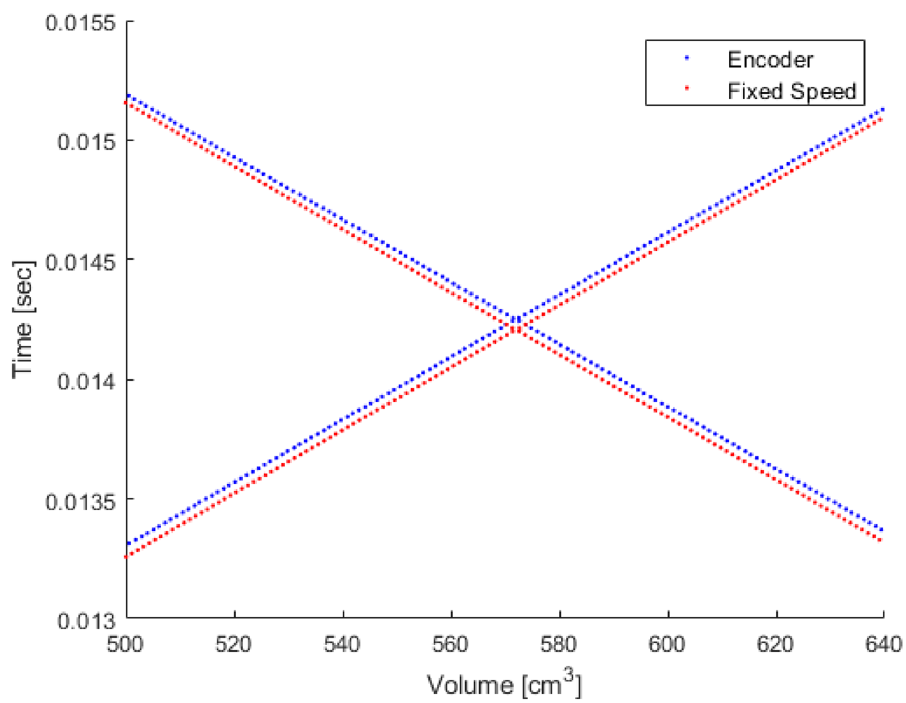

(b) Zoomed in view of volume comparison.

Figure 3.5: Comparison of calculated volume for ,encoder-measured speed, fixed speed, and real speed for the open-drive, R134a, prototype spool compressor presented in Bradshaw et al. (2018).

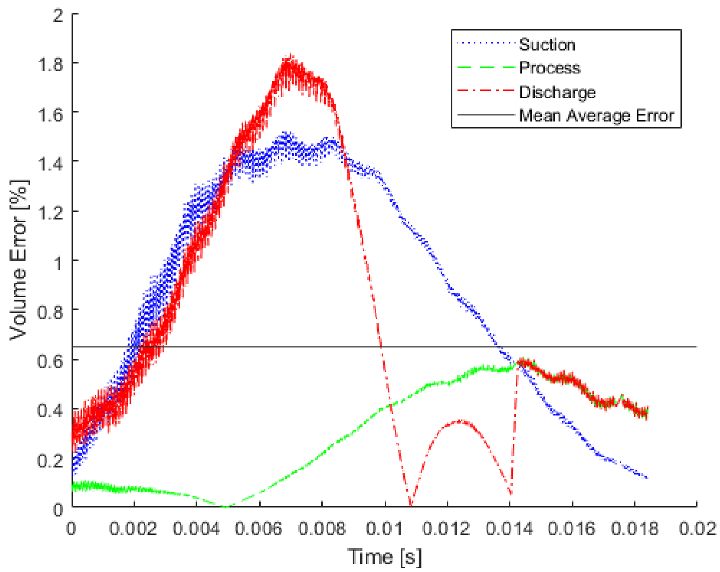

Figure 3.6: Percent error in the volumes between the encoder measured speed and fixed speed for the open-drive, R134a, prototype spool compressor presented in Bradshaw et al. (2018).

for the fixed speed assumption.

3.1.3 Total Boundary Work Uncertainty

The resulting total uncertainty from each of the two sources, volume and pressure, is used as an inputs to an uncertainty propagation analysis for the calculation of the boundary work as calculated following the procedure in Equation 3.6. This analysis results in an error propagation of 0.85% for test condition 8. This method follows ASME-PTC-19.1 (2013) to combine the total uncertainty based on the respective loss expression described in the following sections.

3.2 Ideal loss analysis

The ideal boundary work is an important part of quantifying compressor loss. It's the ideal work done by the system and it used to help quantify loss. Now that pressure and volume have been calculated for each condition,

$$W = -\int P dV$$

is used to find the boundary work. Presented in this section is the process used to evaluate the boundary work calculation for the ideal process of the suction, discharge and compression for test condition 8. Figure 3.7 shows in the ideal indicator diagram to for test condition 8. To ensure the boundary work is correct, each of the ideal processes estimated by hand.

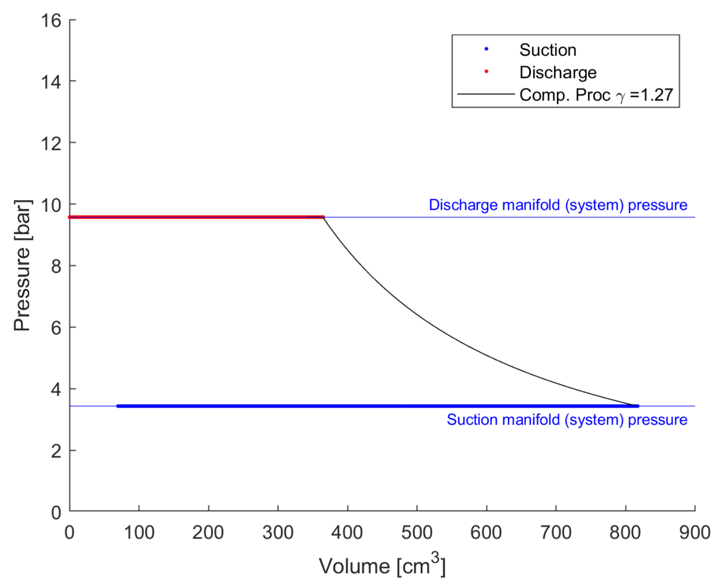

Figure 3.7: Indicator diagram of ideal process for Test condition 8.

For the ideal discharge and suction boundary work the pressure remains constant from start to finish so Equation 3.3 is used for the discharge and Equation 3.4 for the suction. The resulting boundary work for the suction and discharge are shown in Figure 3.8a and Figure 3.8c. The boundary work in the ideal compression has a changing pressure is therefore calculated using a similar method as done in section 3.5. The ideal compression boundary work is shown in Figure 3.8b. To simply verify that the value of the ideal compression process boundary work is in the correct ballpark the areas of a triangle and rectangle are calculated and added together. The triangle and rectangle used for the compression ballpark verification are shown in Figure 3.8d.

$$W_{BW,ideal,dis} = (P_{dis}(V_{dis,start} - V_{min})) \tag{3.3}$$

$$W_{BW,ideal,suc} = (P_{suction}(V_{suc,start} - V_{max})) \tag{3.4}$$

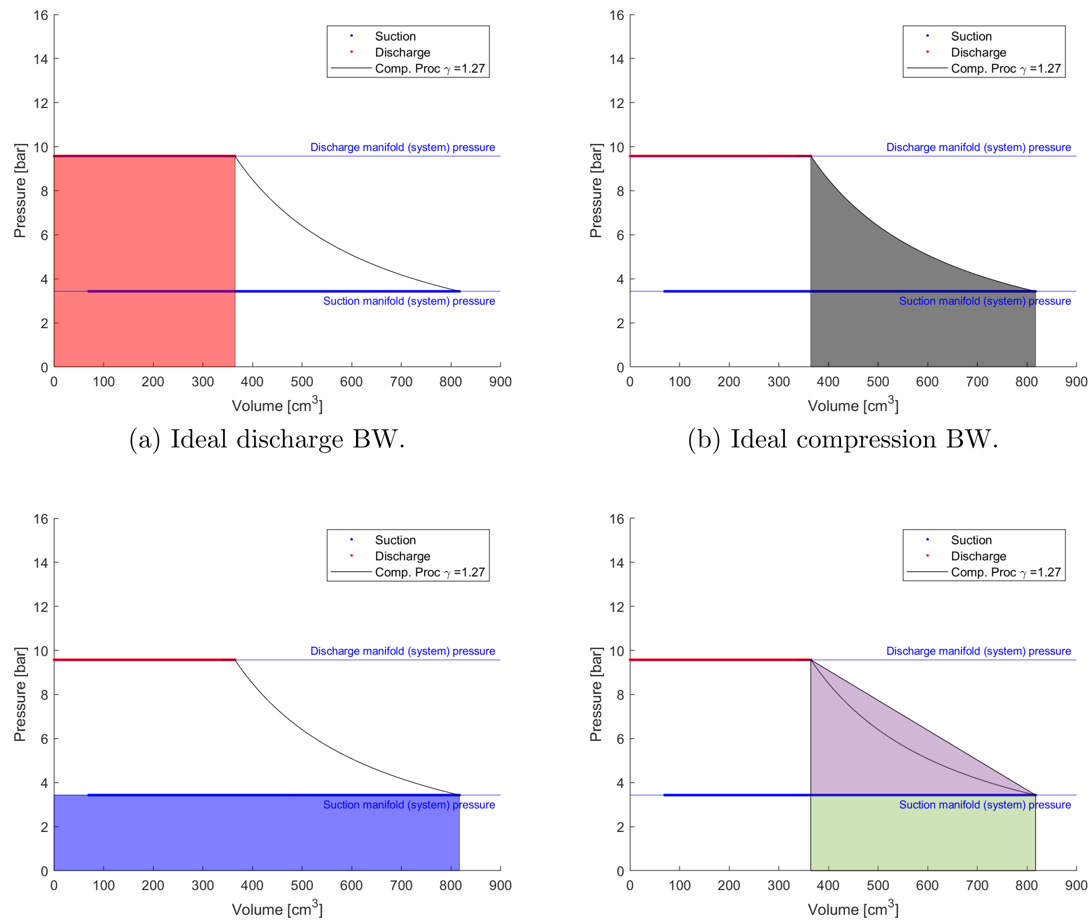

(a) Ideal discharge BW.

(b) Ideal compression BW.

(c) Ideal suction BW.

(d) Compression BW verification.

Figure 3.8: Indicator diagram of ideal processes for Test condition 8 highlighting the ideal boundary work.

Figure 3.9 shows the shaded total ideal boundary work. The compression and discharge boundary work are both taken as positive boundary work as work is being

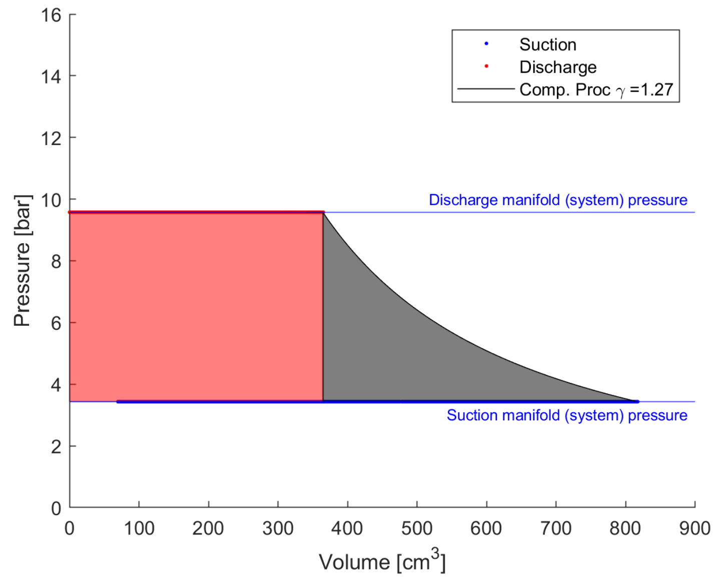

Figure 3.9: Indicator diagram of ideal process for Test condition 8 highlighting the total ideal boundary work.

done while the suction is taken as negative boundary work so the sum of the ideal boundary provides the ideal indicated boundary work calculated as

$$BW_{ideal,total} = W_{BW,ideal,dis} + W_{BW,ideal,comp} - W_{BW,ideal,suc}. \tag{3.5}$$

The following section goes through the calculations of the boundary work loss in the compression, discharge, and suction. The pressure measurements of the actual cycle aren't constant; therefore, numerical methods are used to calculate the boundary work loss. Specifically, the trapezoidal method is used in this work.

3.3 Analysis of discharge loss

The discharge loss is a result of flow losses associated with the discharge port, valves, plenum, and flow into the motor cavity. Pressure drop associated with these areas result in a chamber pressure that is higher than the discharge manifold (system) pressure (p_{dis}) to overcome these losses. This loss is illustrated in Figure 3.10 and is calculated using Equation 3.6 where the chamber pressure is equal to the discharge

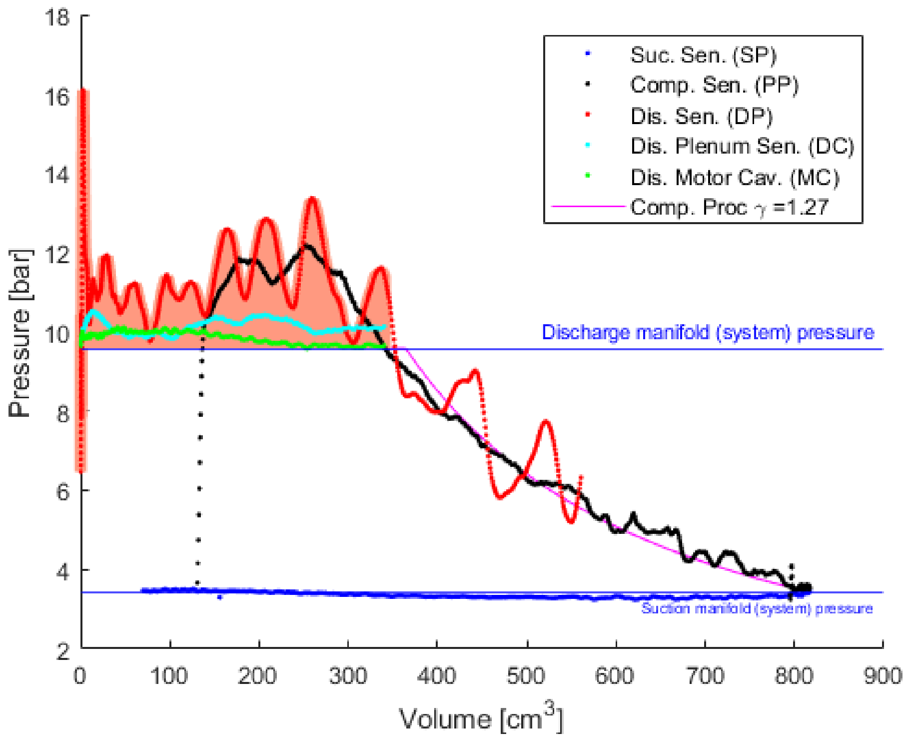

Figure 3.10: Indicator diagram of Test condition 8 highlighting the areas representing the total discharge loss as calculated by Equation 3.6.

chamber (DP) during the discharge process, therefore the total discharge loss is calculated as,

$$L_{discharge} = \underbrace{-\int_{V_{min}}^{V_{dis,start}} p_{DP} dV}_{w_{BW,dis}} - \underbrace{(p_{dis}(V_{dis,start} - V_{min}))}_{w_{BW,dis,ideal}}. \tag{3.6}$$

where the boundary work is integrated using the trapezoidal method between the minimum compression volume and the volume corresponding with the cylinder pressure exceeding the discharge manifold (system) pressure (p_{dis}). The location of the discharge sensor allowed for the entire discharge process to be captured by the discharge sensor.

The discharge loss can be further separated due to the additional pressure transducers in the discharge plenum and motor cavity. These two sensors allow for the discharge loss to be expanded into three separate losses, motor cavity loss, plenum loss, and valve loss. To separately capture the losses associated with the fluid leaving the discharge plenum the same technique is used using pressure data collected from the DC sensor. This assumes that the boundary work required to push fluid from the discharge plenum to the discharge manifold (system) pressure requires the same change in volume as the discharge process itself. Therefore, the total losses from discharge plenum can be evaluated as,

$$L_{dis,plenum} = \underbrace{-\int_{V_{min}}^{V_{dis,start}} p_{DC} dV}_{w_{BW,plenum}} - \underbrace{(p_{dis}(V_{dis,start} - V_{min}))}_{w_{ideal}}. \tag{3.7}$$

Following the same procedure as the discharge plenum, extracting the total losses from the motor cavity to the discharge pipe can be written as,

$$L_{dis,MC} = \underbrace{-\int_{V_{min}}^{V_{dis,start}} p_{MC} dV}_{w_{BW,mc}} - \underbrace{(p_{dis}(V_{dis,start} - V_{min}))}_{w_{ideal}}. \tag{3.8}$$

Finally, taking the difference between the plenum losses and the total discharge losses the remainder is assumed to be dominated by the discharge valves/ports as shown by the shaded portion of Figure 3.11. Therefore, a derived loss is defined to capture this,

$$L_{dis,valves} = L_{discharge} - L_{dis,plenum}. \tag{3.9}$$

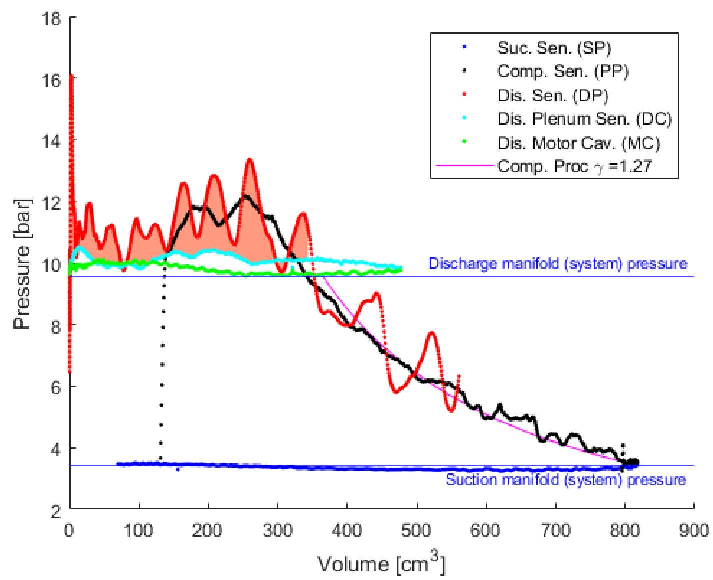

Figure 3.11: Indicator diagram of Test condition 8 highlighting the areas representing the valve loss.

3.4 Analysis of compression losses

The compression process losses are associated with pressure during the closed compression process and calculated relative to an isentropic compression process as shown in Figure 3.12. An isentropic compression process is modeled using a polytropic compression process where the polytropic exponent is assumed to be the ratio of specific heats of the refrigerant calculated at the various suction conditions of the compressor. The general expression to find the loss for the compression process is defined as,

$$L_{comp} = -\int_{V_{max}}^{V_{dis,start}} (p_{PP} - \underbrace{p_{ideal}}_{Ideal Pressure})dV. \tag{3.10}$$

where p_{ideal} is the isentropic compression process found by

$$PV^{\gamma} = const.$$

where gamma is the ratio of specific heats, $V_{dis,start}$ is the volume where the compression stops and discharge process begins, and $V_{max}$is the maximum volume of a single

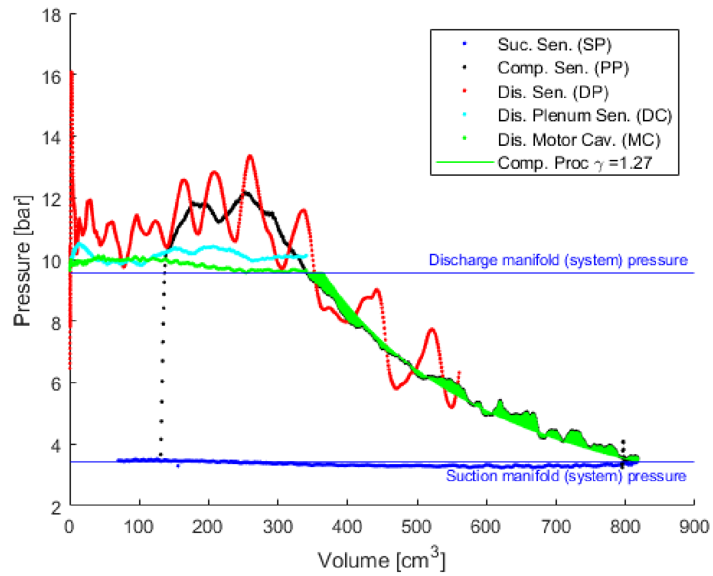

Figure 3.12: Indicator diagram of Test condition 8 highlighting the area representing the compression loss.

compression pocket.

3.5 Analysis of suction losses

Suction losses are associated with flow losses within the suction port as well as leakage that occurs during the suction process. These values are calculated using a similar procedure as the discharge process and shown in Figure 3.13. The loss is therefore given as,

$$L_{suction} = -\int_{V_{max}}^{V_{dis,start}} (p_{SP} - p_{suction})dV. \tag{3.11}$$

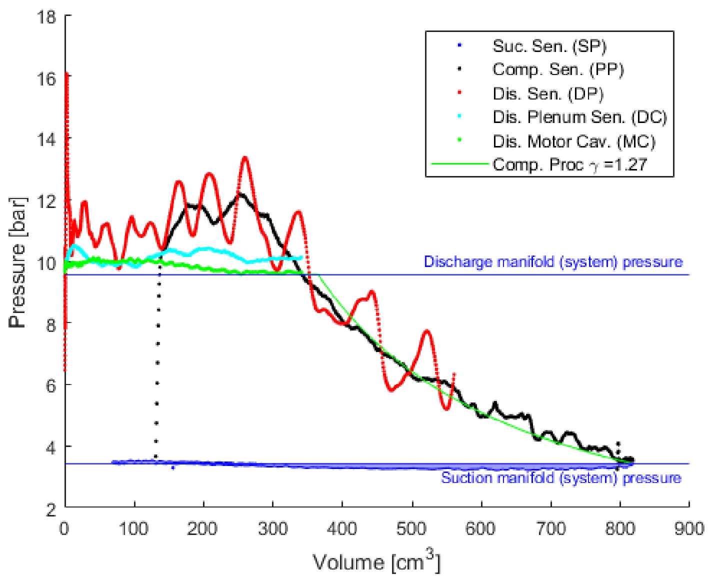

Figure 3.13: Indicator diagram of Test condition 8 highlighting the area representing the suction loss.

CHAPTER IV

RESULTS

This section presents results of the experimental campaign including a detailed breakdown of losses for the 30-ton spool compressor at test condition 8 and an analysis of the trends in the losses. Additionally, the losses are globally analyzed across the breath of conditions presented in the test matrix. Finally, a more detailed analysis of the compression losses is explored. The losses in this section are presented as percentage of total ideal compressor work.

4.1 Loss breakdown at 4.44 °C SST, 37.78 °C SDT, and 1700 rpm (Test condition 8)

Figure 4.1 shows the indicator diagram of operating condition test condition 8. Additionally, the suction manifold (system) pressure, discharge manifold (system) pressure and calculated isentropic work pressure is also overlaid on top of the data as a basis of comparison. The indicator diagram is also presented in Figure 4.2 with the three main loss areas shaded to reflect the calculated loss presented in the previous section. The results of the analysis for test condition 8 are collected in Table 4.1 and broken down by percentage loss associated with each loss mechanism as a percentage of total compressor work.

This table shows that the total discharge loss is by far the largest loss at 18.05% with a portion of that loss being associated with the plenum losses (3.21%) and the motor cavity losses (2.67%), leaving 12.16% of valve losses. Both the plenum and motor cavity losses are significant but neither one is as dominant as the discharge valve losses.

The suction loss (2.67%) reflects the suction pressure measured below the system pressure. Suction loss occurring in this manner is the typical expected loss that occurs at the suction ports. The spool compressor tested doesn't have suction valves; therefore, this loss likely occurs as a result of pressure drop in the suction port.

The compression loss is relatively small despite not qualitatively matching the ideal compression process as shown in Figure 4.1. The measured process is closer to isothermal than the isentropic process (i.e. polytropic exponent is less than specific heat ratio). Therefore, the specific work required is reduced and this results in a 'negative' loss for the portion of the process that approaches the start of the discharge process. This overcomes some of the additional work required to overcome the portion of the process just at the beginning of the compression process. This phenomena is further explored in Chapter 4.3. Overall, the analysis from Test condition 8 suggested that the discharge plenum, motor cavity, and valve losses were the largest in the compressor and should be further explored.

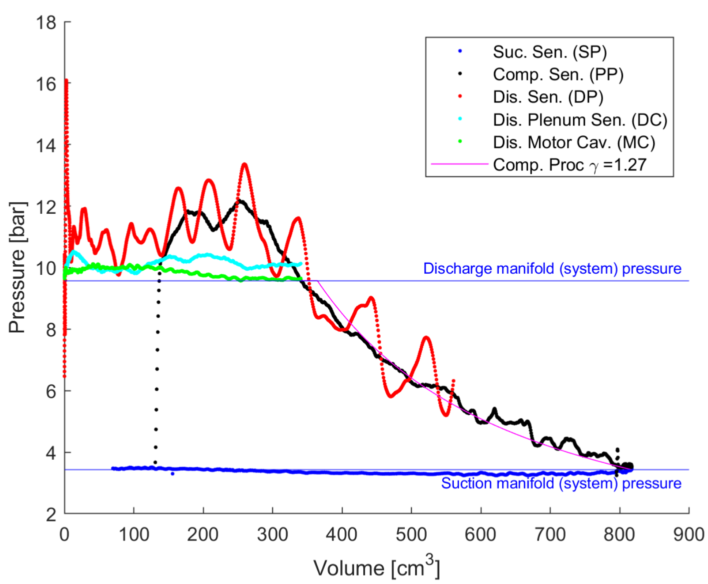

Figure 4.1: Indicator diagram of Test condition 8 with system suction and discharge pressures as well as the estimated isentropic compression process overlaid.

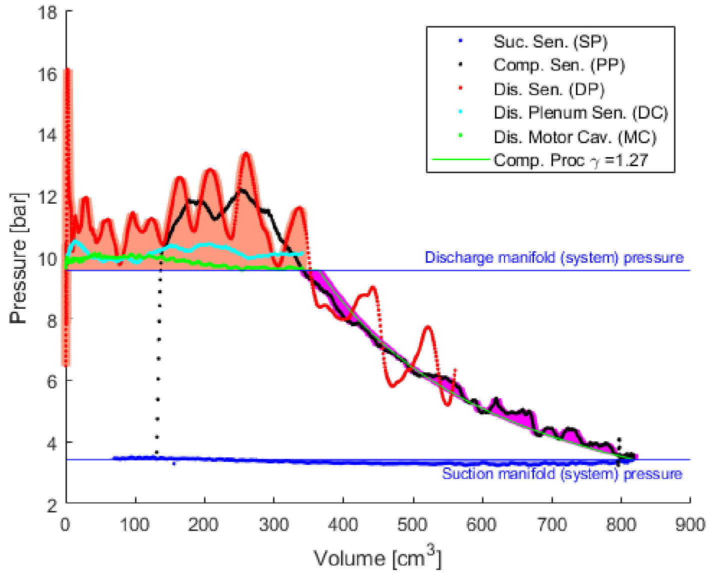

Figure 4.2: Indicator diagram of Test condition 8 with discharge, suction, and compression loss shaded.

Table 4.1: Collection of loss for Test condition 8 presented as a percent of total work.

Test condition 8 Results					
Discharge	**Valves**	**Plenum**	**Motor Cavity**	**Suction**	**Compression**
%	%	%	%	%	%
18.05	12.16	3.21	2.67	1.78	0.68

4.2 Discharge plenum and valve loss

This section will expand on the single operating condition analysis by presenting the suction, compression, discharge, discharge plenum, motor cavity, and valve losses with various operating conditions with an emphasis of the three discharge-related losses.

Figure 4.3 presents the losses for the suction, compression, and discharge (a) and the plenum, motor cavity, and discharge (b) for speeds ranging from 1100 rpm to line voltage (approx. 1750 rpm) compressor shaft speeds at all the SST and SDT reported in Table 2.1. The suction, compression, motor cavity and plenum losses for all the speeds and operating conditions appear to show unremarkable trends. Figure 4.3 highlights that these four losses present with minimal trends with shaft speed. A separate analysis was also explored with SST and SDT and a trend wasn't discovered. The analysis does show a persistent loss of roughly 2-4% for suction, 0-1% for compression, 3-5% for plenum and 1-3% for the motor cavity. The addition of the motor cavity sensor has allowed for this distinction between the flow losses in the plenum and the motor cavity.

In contrast, the valve losses show some significant trends as presented in Figure 4.4. The shaft speed and SDT correlate strongly with the valve loss. The valve loss increases by as much as 5% with speed while the loss decreases by as much as 3% at higher SDT conditions.

It is hypothesized that these losses are associated with either the discharge valves or the valve port/port placement. The valves are generally still not well understood. The magnitude of the results suggest there is still much room for improvement and needs work.

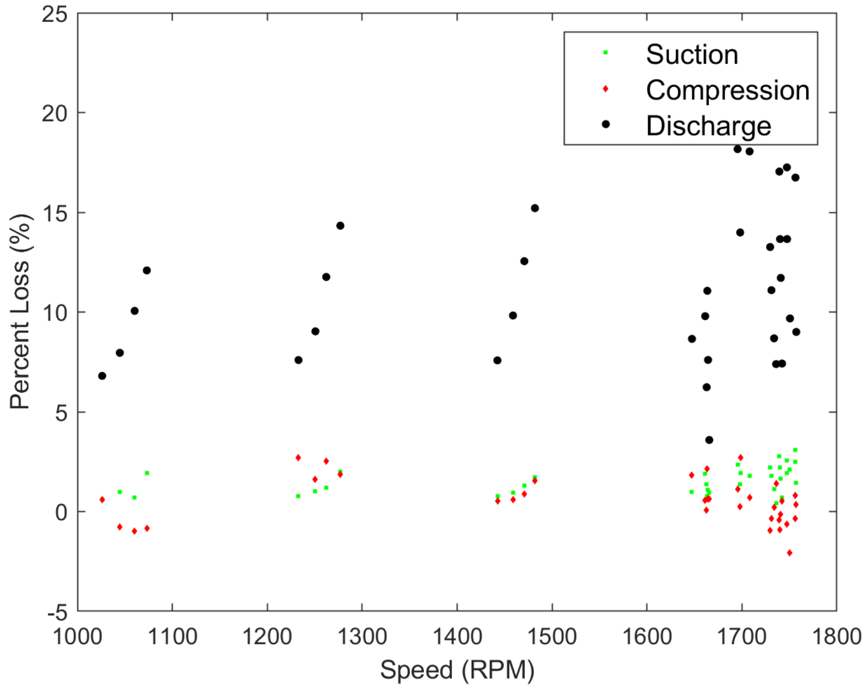

(a) Suction,Compression, and Discharge.

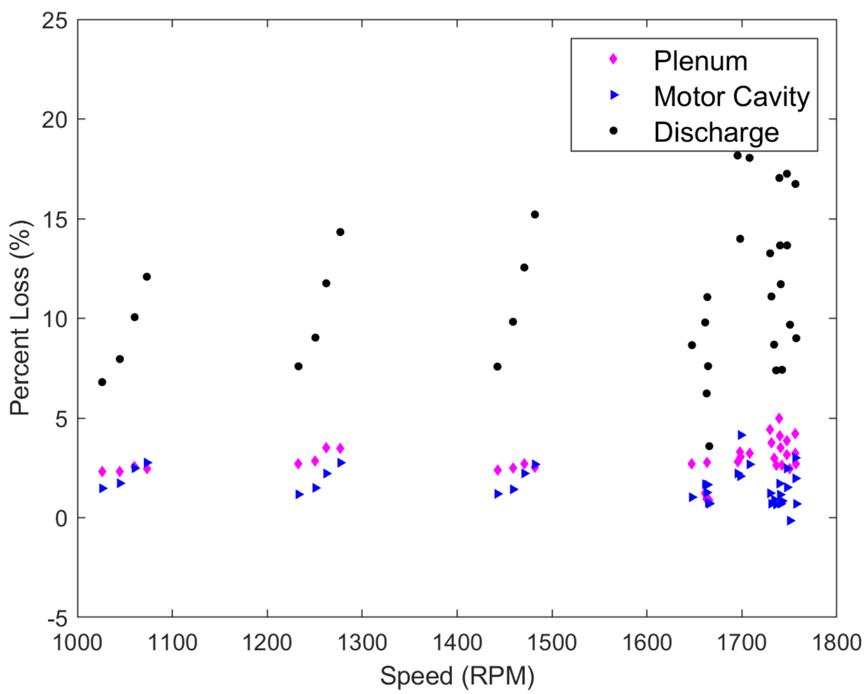

(b) Plenum, Motor Cavity, and Discharge.

Figure 4.3: Indicated discharge plenum, motor cavity and valve losses shown for various speeds (a) and Indicated suction, discharge, and compression losses for various speeds (b). The marker size includes the experimental loss uncertainty.

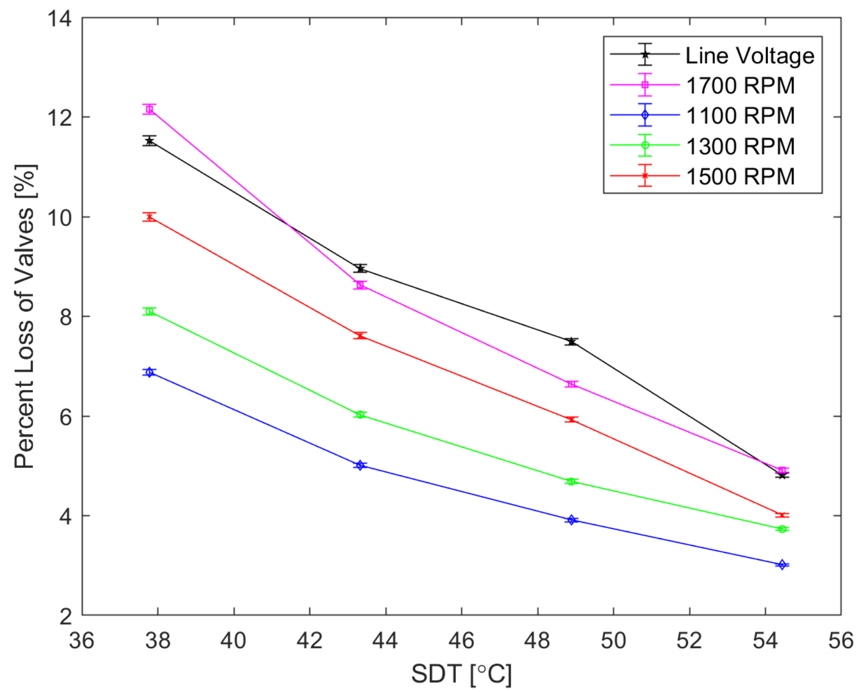

Figure 4.4: Percent Loss of discharge valves v. SDT at a constant 4.4 C (40F) SST for various speeds with error bars

4.3 Compression Process Evaluation

The compression process presents quantitatively low losses but qualitatively high disagreement between the ideal compression processes. This section will further explore this discrepancy by attempting to differentiate between the two mechanisms for loss in an indicated loss (leakage and heat transfer) during this process. If the loss tends to be dominated by leakage this is suggestive that while the quantitative loss value is low, it should still be interpreted as a negative result. In contrast, if heat transfer plays a significant role the quantitatively low result would reflect an appropriately positive result.

To separate heat transfer and leakage an analysis is performed that modifies the ideal isentropic compression processes as an adiabatic compression process with leakage. Adjusting the amount of leakage required for the adiabatic compression to match the measured data for each of the test points in Table 2.1 provides quantification of the amount of mass loss required for the compression process to be adiabatic. The result is a term denoted as IMV (Ideal Mass Volumetric Efficiency) that is compared against the measured volumetric efficiency from each of these tests. If the IMV is lower than the measured volumetric efficiency for a specific data point, it means that the difference in compression process measured cannot be solely explained by leakage. In contrast, if the IMV is higher it suggests that the difference measured could be explained entirely by leakage.

This analysis is accomplished by modifying the ideal compression process model described in Chapter 3.4 with an additional variable ($comp_{leakage}$) that indicates the amount of mass loss in the compression, while still modeling the process as isentropic. This variable is defined as the percentage of mass lost during the compression process,

$$PV^{\gamma} = comp_{leakage}RT. \tag{4.1}$$

For each data point in the test matrix this variable is adjusted until the error between the measured compression process data and the modified ideal compressor process is minimized. The final ($comp_{leakage}$), variable for each point is converted to a percentage of total starting mass which is defined as,

$$IMV = 1 - comp_{leakage}. \tag{4.2}$$

This definition allows a direct comparison between the measured volumetric efficiency of the compressor and IMV, the results are presented in Figure 4.5. If the mass volumetric loss taken from the volumetric efficiency matches or is greater than that of the IMV than this suggests that the majority of the loss in the compression process can be attributed as loss due to leakage. If the mass loss represented is less, then leakage cannot solely account for the differences in the compression process and heat transfer must be a contributing factor.

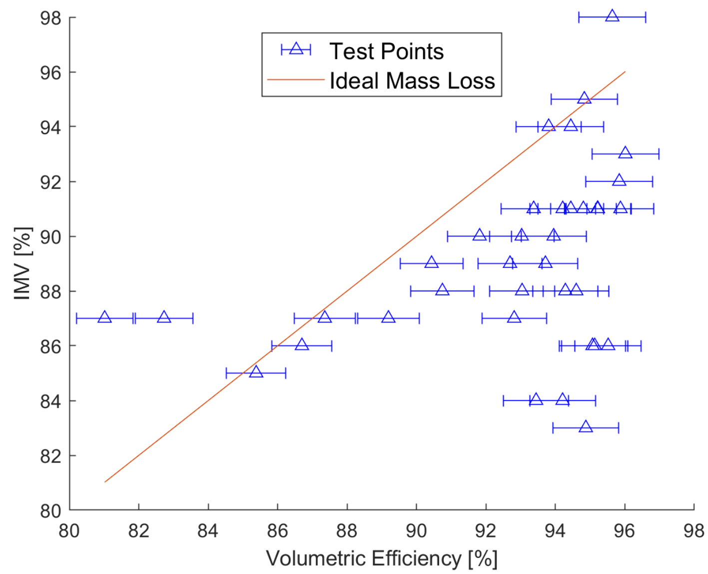

Figure 4.5: Mass loss compared against measured volumetric efficiency.

As Figure 4.5 shows, there are 25 out of the 36 data points where the differences in compression process cannot be solely explained by leakage. This suggests that this compressor architecture has a meaningful amount of heat rejection from the compression chamber and may be suitable for additional modifications, such as liquid/vapor injection to further increase efficiency.

CHAPTER V

CONCLUSIONS AND FUTURE WORK

5.1 Conclusions

This thesis presents an indicated loss analysis that is part of the work that will be used in conjunction with additional data presented in Appendix D for the development of a new spool compressor design for the next generation refrigerants. The indicated loss analysis is performed on the 8^{th} generation, 30-ton, prototype spool compressor. The losses were collected using high-speed pressure measurements from five locations within the compressor and synchronized with a proximity sensor as the trigger mechanism. The results suggest that the largest economical opportunity for improvement in this prototype is a re-design of the discharge plenum. This re-design has the potential to result in 3-4% improvement in the overall compressor efficiency. Additionally, a redesign of the motor cavity could add an additional potential improvement of 2-3%. The valve losses presented an increasing trend with increasing speed and decreasing SDT. This trend is believed to be as result of changing mass flow rate and change in valve dynamics due to the pressure change across the valves. The valve improvements presented are the largest potential improvement with losses ranging from 9-18% depending on speed and operating condition. The valve losses presented as somewhat independent of suction conditions but relatively sensitive to discharge condition. The indicated losses of the valves indicate that more study of the dynamics of the valves is necessary to ensure the losses are mitigated across the entire operating range. Additionally, the flow losses into the valve ports could be reduced by redesigning the valve port entrance.

Finally, the compression loss was evaluated in an attempt to differentiate between the influence of leakage and heat transfer. It was concluded that for 25 of the 36 operating conditions, leakage can't entirely be concluded as the primary cause of compression losses. Therefore, heat transfer likely plays a significant role in the compression loss. This is generally not the case with most compressors and may be a result of a compressor architecture. The additional effect due to heat transfer suggests that this compressor architecture may be suitable for enhancements such as flooded compression as a means to further improve efficiency.

5.2 Future Work

The four major contributing losses found were the valve loss, plenum loss, motor cavity loss, and compression loss. Redesigning the plenum and flow through the motor cavity of the compressor can aid in reducing the flow losses. Further evaluation of the flow losses of the the compressor with the utilization of computational fluid dynamics (CFD) could aid in the effectiveness of the redesign of the plenum, motor cavity and the discharge valve porting. Using the data presented in this loss analysis could allow for a CFD model to be validated and effectually used to see visual the flow losses with redesigns. Additionally, the discharge valves indicate that further study of the dynamics could be done with comprehensive value model development. Further macro analysis of the 40 ton spool compressor has been done following this work and is shown in Appendix D. The additional steady state data along with the dynamic loss analysis should be used to improve the comprehensive model to allow for better predictions of new compressor design with new generation refrigerants.

REFERENCES

ASHRAE-23.1 (2010). Methods of Testing for Rating the Performance of Positive Displacement Refrigerant Compressors and Condensing Units That Operate at Subcritical Temperatures. Technical report, American Society of Heating, Refrigeration, and Air Conditioning Engineers.

ASME-PTC-19.1 (2013). Test uncertainty.

Bauer, F. (1988). Valve losses in reciprocating compressors. In *International Compressor Engineering Conference*, No.631.

Bianchi, G. and Cipollone, R. (2015). Theoretical modeling and experimental investigations for the improvement of the mechanical efficiency in sliding vane rotary compressors. *Applied Energy*, 142:95–107.

Bradshaw, C. (2013). Spool compressor tip seal design considerations. In *8th International Conference on Compressors and their Systems*, pages 1–10.

Bradshaw, C. R. and Groll, E. A. (2013). A comprehensive model of a novel rotating spool compressor. *International Journal of Refrigeration*, 36(7):1974–1981.

Bradshaw, C. R., Kemp, G., Orosz, J., and Groll, E. A. (2016). Development of a loss pareto for a rotating spool compressor using high-speed pressure measurements and friction analysis. *Applied Thermal Engineering*, 99:392–401.

Bradshaw, C. R., Kemp, G., Orosz, J., and Groll, E. A. (2018). An Indicated Loss Analysis of a Light-Commercial Spool Compressor using High-Speed Pressure Measurements. In *International Compressor Engineering Conference*, 2555, pages 1–10.

DOE (2011). 2010 Buildings Energy Data Book. Technical report, U.S. Department of Energy.

EIA (2011). Electric power monthly. Technical report, U.S. Energy Information Administration. Retrieved July 3, 2020 **URL**: `https://www.eia.gov/totalenergy/data/monthly`.

Haugland, K. (1990). Pressure Indication of Twin Screw Compressor_1990.pdf. In *International Compressor Engineering Conference*, No .735.

Huang, G., Shen, X., and Yan, Z. (2018). Experimental Study on P-V diagram and motion curve of suction and discharge valve in reciprocating compressor. In *International Compressor Engineering Conference*, No. 2586, pages 1–10.

Huang, Y. M. and Yang, S. A. (2008). A measurement method for air pressures in compressor vane segments. *Measurement: Journal of the International Measurement Confederation*, 41(8):835–841.

Jacobs, J. J. (1976). Analytic and experimental techniques for evaluating compressor performance losses. In *International Compressor Engineering Conference*, No.179.

Kemp, G., Garrett, N., and Groll, E. A. (2008). Novel Rotary Spool Compressor Design and Preliminary Prototype Performance. In *International Compressor Engineering Conference*, Paper 1866., pages 1–10.

LabVIEW (2013). *Version 13.0.1.* National Instruments, Austin, Texas.

MATLAB (2020). *Version 9.9.0 (R2020b).* The MathWorks Inc., Natick, Massachusetts.

Nikolov, A. and Brümmer, A. (2016). Analysis of Indicator Diagrams of a Water Injected Twin-shaft Screw-type Expander. In *International Compressor Engineering Conference*, pages 1–10.

Nomura, T., Ohta, M., Takeshita, K., and Ozawa, Y. (1984). Efficiency improvement in rotary compressor. In *International Compressor Engineering Conference*, Paper 468, pages 1–9.

Orosz, J., Bradshaw, C. R., Kemp, G., and Groll, Eckhard, A. (2016). Updated Performance and Operating Characteristics of a Novel Rotating Spool Compressor. In *International Compressor Engineering Conference*, Paper 2467., pages 1–9.

Orosz, J., Bradshaw, C. R., Kemp, G., and Groll, E. (2012). Updated Performance and Operating Characteristics of a Novel Rotating Spool Compressor. In *International Compressor Engineering Conferences*, pages 1–9.

Orosz, J., Kemp, G., Bradshaw, C. R., and Groll, E. A. (2014). Performance and Operating Characteristics of a Novel Rotating Spool Compressor. In *International Compressor Engineering Conference*, Paper 2327., pages 1–9.

Peng, X., Xing, Z., Cui, T., and Li, L. (2002). Analysis of the working process in an oil-flooded screw compressor by means of an indicator diagram. *Proceedings of the Institution of Mechanical Engineers, Part A: Journal of Power and Energy*, 216(6):465–470.

Real, M. A. R. and Pereira, E. A. G. (2010). Using PV Diagram Synchronized With the Valve Functioning to Increase the Efficiency on the Reciprocating Hermetic Compressors. In *International Compressor Engineering Conference*, No. 1966, pages 1–8.

Rigola, J., Perez-Segarra, C. D., Raush, G., Oliva, A., Escriba, M., Jover, J., and Escanes, F. (2002). Experimental Studies Of Hermetic Reciprocating Compressors With Special Emphasis On pV Diagram. In *International Compressor Engineering Conference*, No.1506, pages 1–10.

Schmidt, D., Singleton, J., and Bradshaw, C. (2019). Development of a light-commercial compressor load stand to measure compressor performance using low-GWP refrigerants. *International Journal of Refrigeration*, 100.

Singleton, J. M. (2020). *Control and Commissioning of a Hot-Gas Bypass Compressor Load Stand for Testing Light-Commercial Compressors Using Low-GWP Refrigerants.* Masters thesis, Oklahoma State University.

Stošic, N., Milutinović, L., Hanjalić, K., and Kovačević, A. (1992). Investigation of the influence of oil injection upon the screw compressor working process. *International Journal of Refrigeration*, 15(4):206–220.

Westphalen, D. and Koszalinski, S. (2001). *Energy Consumption Characteristics of Commercial Building HVAC Systems Volume I : Chillers, Refrigerant Compressors and Heating Systems.*

Wood, N., Bradshaw, C. R., Orosz, J., Kemp, G., and Groll, Eckhard, A. (2016). Dynamic Modeling of a Poppet Valve for use in a Rotating Spool Compressor. In *International Compressor Engineering Conference*, No. 2468, pages 1–9.

Yang, B., Peng, X., He, Z., Guo, B., and Xing, Z. (2009). Experimental investigation on the internal working process of a CO2 rotary vane expander. *Applied Thermal Engineering*, 29(11-12):2289–2296.

APPENDICES

APPENDIX A: Single Condition Matlab Code

```matlab
%%
tic
clear
clc
close all
set(0,'DefaultFigureWindowStyle','docked')
un=units;                               %Allows easy unit changing
%% Inputs
%Select Test Condition Number
opcond_num = 8;
Testdata = uigetdir ;
myFolder = strcat(convertCharsToStrings(Testdata),'\',num2str(opcond_num));
buildsheet = uigetfile ;                  %build file name of test load stand
testmatrix = uigetfile ;                  %select test matrix

alpha = 0;                              %degrees triggered at TDC so there is no offset
zulu = 0;                               %degrees offset in case trigger was off from TDC
% Pressure Sensor width 3.4 degrees
theta_SP2 = 90.0+zulu;                  %Suction Sensor Location
theta_PP1 =249.0-1.7+zulu;              %upstream process pocket location
theta_PP2 = theta_PP1+3.4;              %downstream process pocket location
theta_DP1 = 345.8-1.7+zulu;             %upstream discharge pocket location
theta_DP2 = theta_DP1+3.4;              %downstream discharge pocket location
build_file = buildsheet;
test_mtx = testmatrix;
only_180 = true;                        %determine if going to use the entire
```

```
                                              %cycle or only half cycle
debug = true;                                 %debug flag to show plots which are helpful

%% Collect bulk data from build files
[numbld]=xlsread(build_file);
ind_op_cond = find(numbld(:,1)==opcond_num); %Finds the correct row of data...
%for the desired test condition.
SST = numbld(ind_op_cond,49);         %[F]
SDT = numbld(ind_op_cond,50);         %[F]
Power = numbld(ind_op_cond,51);      %refers to whether or not line voltage is used.
P_dis_bulk = numbld(ind_op_cond,4);  %[psi]
P_suc_bulk = numbld(ind_op_cond,5);  %[psi]
T_suc_bulk = numbld(ind_op_cond,3);  %[F]
T_dis_bulk = numbld(ind_op_cond,4);  %[F]
M_dot = numbld(ind_op_cond,7);       %[lbm/min]
T_shell1 = numbld(ind_op_cond,36);   %[F]
T_shell2 = numbld(ind_op_cond,37);   %[F]
P_amb = numbld(ind_op_cond,14);      %[psi]
Speed_bulk = numbld(ind_op_cond,41); %[rpm]
W_dot_elec = numbld(ind_op_cond,16); %[kW]

%% Collect data from high-speed data files
%Select folder at the top of this file
%Check to make sure that folder actually exists.  Warn user if it doesn't.
if ~isfolder(myFolder)
  errorMessage = P_4_avgrintf('Error: The following folder does not exist:\n%s', myFolder);
  uiwait(warndlg(errorMessage));
  return;
end
% Get a list of all files in the folder with the desired file name pattern.
csvFiles = dir(fullfile(myFolder, '*.csv'));
numFiles = length(csvFiles);
startRow= 16;   %Starts reading from the row where it first sees a number.
endRow = 3200;  %End row that covers at least a full rotation for all conditions.

%Preallocation to make code run faster.
rowcount=endRow-(startRow-1);
```

```
Speed = zeros(rowcount,numFiles);
Time  = zeros(rowcount,numFiles);
Angle = zeros(rowcount,numFiles);
Temp  = zeros(rowcount,numFiles);
P_1   = zeros(rowcount,numFiles);
P_2   = zeros(rowcount,numFiles);
P_3   = zeros(rowcount,numFiles);
P_4   = zeros(rowcount,numFiles);
P_5   = zeros(rowcount,numFiles);

%Reads in the data from each csv file assigning the data to a new column
%for each file.
for k = 1 : numFiles
  Read_files = xlsread(fullfile(myFolder,csvFiles(k).name));
  Time(:,k)  = Read_files(startRow:endRow,1);
  Angle(:,k) = Read_files(startRow:endRow,2);
  Temp(:,k)  = Read_files(startRow:endRow,3); %Top of motor temp
  P_1(:,k)   = Read_files(startRow:endRow,4); %Suction Port
  P_2(:,k)   = Read_files(startRow:endRow,5); %Process Port
  P_3(:,k)   = Read_files(startRow:endRow,6); %Plenum Port
  P_4(:,k)   = Read_files(startRow:endRow,7); %Discharge Port
  P_5(:,k)   = Read_files(startRow:endRow,8); %Motor Cavity
end

%Takes the averages of each column and converts to absolute pressure.
SP_avg=mean(P_1, 2)+P_amb;  %[psi]
PP_avg=mean(P_2, 2)+P_amb;  %[psi]
DC_avg=mean(P_3, 2)+P_amb;  %[psi]
DP_avg=mean(P_4, 2)+P_amb;  %[psi]
MC_avg=mean(P_5, 2)+P_amb;  %[psi]
Temp_avg=mean(Temp, 2);     %[F]
Time_avg=mean(Time, 2);     %[sec]
Ang_avg=Time_avg .*(Speed_bulk*6); %[degrees](360/60)

%%Get Volume for each sensor.

%Inputs for geometric model
%number of points requested from base geometry
num_pts = round(((70000*30)/(Speed_bulk)),0);
%70K sampmes/sec *min/1700ish rev * 60sec/min * 1/2rev = sample/rev
%collect input and geometry objects from Bradshaw(2016) model
```

```
. Not
%attached.
[ c, sgo ] = collect_geometry( num_pts );

%Preallocate for volumes.
VSP = zeros(1,length(Ang_avg));
VPP = zeros(1,length(Ang_avg));
VDP = zeros(1,length(Ang_avg));
VDC = zeros(1,length(Ang_avg));
VMC = zeros(1,length(Ang_avg));

%Checking these two to try to cover the entire suction process.
%Unused currently
VSP_2 = zeros(1,length(Ang_avg));
VSP_3 = zeros(1,length(Ang_avg));

%calculate vector of thetas based on input theta
theta_double = [sgo.theta_plot(1:end-1)-alpha*(un.deg/un.rad), ...
    sgo.theta_plot(1:end-1)+pi-alpha*(un.deg/un.rad),sgo.theta_plot...
    +2*pi-alpha*(un.deg/un.rad)];
V_double = [sgo.V(1:end-1,:); sgo.V(1:end-1,:); sgo.V];
Vinterp = interp1(theta_double,V_double,Ang_avg*(un.deg/un.rad));

for kk = 1:1:length(Ang_avg)
    %suction sensor
    if Ang_avg(kk) >= theta_SP2 && Ang_avg(kk) < 180 || Ang_avg(kk) >= ...
            theta_SP2 + 180 && Ang_avg(kk) < 360
        VSP(kk) = Vinterp(kk,1); %suction pocket
    else
        VSP(kk) = Vinterp(kk,2);  %compression process
    end
     %compression sensor
    theta_pp_avg = ((theta_PP1 + theta_PP2)/2)- 180;
    if Ang_avg(kk) >= theta_pp_avg && Ang_avg(kk) < 180 || Ang_avg(kk) >= ...
            theta_pp_avg + 180 && Ang_avg(kk) < 360
        VPP(kk) = Vinterp(kk,2); %compression pocket
    else
        VPP(kk) = Vinterp(kk,3);  %discharge process
    end
```

```
    %discharge sensor
    theta_dp_avg = ((theta_DP1 + theta_DP2)/2)- 180;
    if Ang_avg(kk) <= theta_dp_avg && Ang_avg(kk) < 180 || Ang_avg(kk) >= ...
            theta_dp_avg + 180 && Ang_avg(kk) < 360
        VDP(kk) = Vinterp(kk,3);
    else
        VDP(kk) = Vinterp(kk,2);
    end
    VDC(kk) = Vinterp(kk,3);
    VMC(kk) = Vinterp(kk,3);
end

%Full 360 degree rotation
    ind_ang360 = find(Ang_avg>=360,2);
    Ang_avgFL = Ang_avg(1:ind_ang360);
    SP_avgFL = SP_avg(1:ind_ang360);
    PP_avgFL = PP_avg(1:ind_ang360);
    DP_avgFL = DP_avg(1:ind_ang360);
    DC_avgFL = DC_avg(1:ind_ang360);
    MC_avgFL = MC_avg(1:ind_ang360);
%Half Rotation
if only_180
    ind_ang180 = find(Ang_avg>=180,2);
    Ang_avg = Ang_avg(1:ind_ang180);
    SP_avg = SP_avg(1:ind_ang180);
    PP_avg = PP_avg(1:ind_ang180);
    DP_avg = DP_avg(1:ind_ang180);
    DC_avg = DC_avg(1:ind_ang180);
    MC_avg = MC_avg(1:ind_ang180);
    VSP = VSP(1:ind_ang180);
    VPP = VPP(1:ind_ang180);
    VDP = VDP(1:ind_ang180);
    VDC = VDC(1:ind_ang180);
    VMC = VMC(1:ind_ang180);
end

%% Loss calcs

%First find indices for points 1-4
%point 1 being the start of the suction, point 2 being start of
%compression, point three being start of discharge, point 4 being end of
```

```
%discharge.

%Indices 1 and 2 are found in the suction losses portion.
%Indices 3 and 4 are found in the discharge.
ind_dis = find(PP_avg>=P_dis_bulk,1);
ind_dis_dp = find(DP_avg>=P_dis_bulk);

if ~isempty(ind_dis)
    V_dis_start = VPP(ind_dis); %volume that discharging starts
else %use discharge pocket signal
    V_dis_start = VDP(ind_dis_dp); %volume that discharging starts
end
ind_dp_vol = find(VDP == V_dis_start); %Volume Index 3 at discharge start.

if isempty(ind_dp_vol)
    %this means that the discharge process data does not drop below bulk
    %discharge pressure, need to add a layer between them.
    ind_dp_maxDP = find(VDP == max(VDP)); %index of max volume
    %use this and ind_dis to create extra range
    ind_dp_vol = ind_dis;
end

ind_dp_vol2 = find(VDP == min(VDP)); %Index 4 discharge minimum volume

%% Calculate the discharge losses from indeces 3 to 4
    BWd1 = -trapz(VDP(ind_dp_vol:ind_dp_vol2),DP_avg(ind_dp_vol:ind_dp_vol2)...
        *(un.psi/un.Pa));
    %add in BW calculation for cover sensor
    BWd1_c = -trapz(VDP(ind_dp_vol:ind_dp_vol2),DC_avg(ind_dp_vol:ind_dp_vol2)...
        *(un.psi/un.Pa));
    %Boundary Work for Motor Cavity Sensor
    BWd1_mc = -trapz(VDP(ind_dp_vol:ind_dp_vol2),MC_avg(ind_dp_vol:ind_dp_vol2)...
        *(un.psi/un.Pa));

    %Verfies dishcharge line is correct.
    if debug
```

```
        figure('name','Discharge loss indeces line')
        plot(VDP(ind_dp_vol:ind_dp_vol2)*(un.m3/un.cc),DP_avg(ind_dp_vol:...
          ind_dp_vol2)*(un.psi/un.bar),'b--','linewidth',3)
        hold on
        plot(VDP*(un.m3/un.cc),DP_avg*(un.psi/un.bar),'g.')
        title('Discharge Indeces Line')
        xlabel('Volume [cm^3]')
        ylabel('Pressure [Bar]')
        legend('Discharge Loss Line','Entire Discharge Line')
        hold off
    end
%end
BWd = BWd1 ;  %[Pa*m^3 or J or N-m] Discharge BW
 BWd_p = BWd1_c ; %[Pa*m^3 or J or N-m] Plenum + MC BW
 BWd_mc = BWd1_mc ; %[Pa*m^3 or J or N-m]                    Motor Cavity BW
%Calculate ideal discharge Boundary Work %[Pa*m^3 or J or N-m]
 BW_ideal = P_dis_bulk*(un.psi/un.Pa)*(V_dis_start - min(VDP));


%Losses %[Pa*m^3 or J or N-m]
 Loss_dis = BWd - BW_ideal;

 Loss_mc= BWd - BWd_mc; %[Pa*m^3 or J or N-m]          Plenum and Valves loss
 Loss_valves= BWd - BWd_p; %[Pa*m^3 or J or N-m] Valve BW Loss
 Loss_plenum= BWd_p - BWd_mc; %[Pa*m^3 or J or N-m] Plenum only BW Loss
 Loss_dis_pmc = BWd_p - BW_ideal; %Plenum + MC Loss
 Loss_dis_mc = BWd_mc - BW_ideal; %Motor Cavity Percent Loss
 Loss_vp = Loss_dis - Loss_dis_mc; %Loss of vavles + plenum


%%%%%%%%%%%%%%
%% Suction Losses
%%%%%%%%%%%%%%

%Find important indicies
%Indices 1 and 2
```

```
[A,idx] = sort(VSP);

ind_sp_min_vol = idx(2); %index of minimum suction volume
ind_pp_max_vol = find(VPP==max(VPP),1); %index of maximum volume in VPP
ind_pp_min_vol = find(VPP==min(VPP),1); %index of minimum volume in VPP
ind_sp_max_vol = find(VSP==max(VSP),1); %index of max suction volume
%Rearrange Suction Pressure and Volume into a single
VSP_combined = [VSP(ind_sp_min_vol:end-3) VSP(1:ind_sp_max_vol)];
SP_avg_combined = [SP_avg(ind_sp_min_vol:end-3); SP_avg(1:ind_sp_max_vol)];
if ind_sp_min_vol > 1
    %Calculate suction boundary work
    BWsuc1 = trapz(VSP(ind_sp_min_vol:end),SP_avg(ind_sp_min_vol:end)*(un.psi/un.Pa)) +...
    trapz(VSP(1:ind_sp_max_vol),SP_avg(1:ind_sp_max_vol)*(un.psi/un.Pa));
    Bwsuc_singleline = trapz(VSP_combined,SP_avg_combined*(un.psi/un.Pa));
    V_suc_start = VSP(ind_sp_min_vol);
else %if not, suction starts at zero
    BWsuc1 = trapz(VSP(1:end),SP_avg(1:end)*(un.psi/un.Pa));
    V_suc_start = VSP(1);
end
%Verify
if debug
    figure('name','Suction Loss debug')
    plot(VSP(ind_sp_min_vol:end-3)*(un.m3/un.cc),(SP_avg(ind_sp_min_vol:end-3))...
      *(un.psi/un.bar),'g')
    hold on
    plot(VSP(1:ind_sp_max_vol)*(un.m3/un.cc),(SP_avg(1:ind_sp_max_vol))*...
      (un.psi/un.bar),'r')
    %plot(VSP*(un.m3/un.in3),SP_avg,'b.')
    plot(VSP_combined*(un.m3/un.cc),SP_avg_combined*(un.psi/un.bar),'k--')
    %plot(VPP(1:ind_pp_max_vol)*(un.m3/un.in3),PP_avg(1:ind_pp_max_vol),'k-')
    hold off
end
%index of max volume observed by SP sensor based on VPP
```

```
ind_pp_start_vol = find(VPP == max(VSP));
V_suc_end = VSP(ind_sp_max_vol);

%Only uses the suction sensor
BWsuc = BWsuc1; %total BW for suction process
%ideal BW
BWsuc_ideal = -P_suc_bulk*(un.psi/un.Pa)*(V_suc_start - V_suc_end); %also in N-m
BWsuc_start = -P_suc_bulk*(un.psi/un.Pa)*(0-V_suc_start); % section of ...
%suction BW not accounted for.

%loss calculations
Loss_suc= BWsuc_ideal - BWsuc ;


%% Compression Losses

%need to integrate from ind_pp_max_vol:ind_dp_vol
%if ind_dp_vol == ind_dis then process pocket data can be used all the way
%if ind_dp_vol == ind_dis_dp then process pocket data cannot be used for
%entire calculation and need to find where they split off

%find indexes for start and end of compression.
ind_pp_maxP = find(PP_avg == max(PP_avg));
ind_pp_dis=VPP(ind_dis);
ind_pp_dis_vol = find(VPP== ind_pp_dis);
%then integrate from ind_pp_max_vol:ind_pp_maxP +
%ind_pp_maxP:ind_dp_vol

%Find Cp and Cv using EOS to get gamma
Cp = EOS('C','T',convtemp2(T_suc_bulk,'F','K'),'P',P_suc_bulk*(un.psi/un.Pa)...
    ,'R134a','CoolProp');
Cv = EOS('O','T',convtemp2(T_suc_bulk,'F','K'),'P',P_suc_bulk*(un.psi/un.Pa)...
    ,'R134a','CoolProp');
gamma = Cp/Cv;

%Creating a single array with the process sensor volume and pressure made
%into an array in the correct order
VPP_combined = [VPP(ind_pp_max_vol:end-2) VPP(1:ind_dp_vol)];
```

```
PP_avg_combined = [PP_avg(ind_pp_max_vol:end-2); PP_avg(1:(ind_dp_vol))];
PP_length=length(PP_avg_combined);
%Allocated for speed.
P_comp_ideal = P_suc_bulk*ones(1,PP_length);

if debug
    figure('name','Compression Process Debug')
    %plot(VPP(ind_pp_max_vol:ind_dp_vol)*(un.m3/un.cc),...
    %(PP_avg(ind_pp_max_vol:ind_dp_vol))*(un.psi/un.bar))
    plot(VPP(1:ind_dp_vol)*(un.m3/un.cc),(PP_avg(1:ind_dp_vol))*(un.psi/un.bar),'r')
    %plot(VPP(ind_dp_vol:end)*(un.m3/un.cc),(PP_avg(1:ind_dp_vol))*(un.psi/un.bar))
    hold on
    plot(VPP(ind_pp_max_vol:end)*(un.m3/un.cc),(PP_avg(ind_pp_max_vol:end))...
        *(un.psi/un.bar),'g')
    plot(VPP(ind_dp_vol)*(un.m3/un.cc),(PP_avg(ind_dp_vol))*(un.psi/un.bar),'kd')
    plot(VPP(ind_pp_max_vol)*(un.m3/un.cc),(PP_avg(ind_pp_max_vol))*...
        (un.psi/un.bar),'kd')
    plot(VPP_combined *(un.m3/un.cc),PP_avg_combined*(un.psi/un.bar),'k:',...
        'linewidth',1)
    hold off
    legend('1-line end','max_pp_vol-end','indeces 3','indeces 2')
    xlabel('Volume [cc^3]')
    ylabel('Pressure [bar]')
end

if ind_dp_vol == ind_dis %if true then PP_avg is available all the way through process
    BWcomp = -trapz(VPP(1:ind_dp_vol),PP_avg(1:ind_dp_vol)*(un.psi/un.Pa))+...
        -trapz(VPP(ind_pp_max_vol:end),PP_avg(ind_pp_max_vol:end)*(un.psi/un.Pa));
    BWcomp_singleline = -trapz(VPP_combined,PP_avg_combined*(un.psi/un.Pa));

    %Ideal compresssion process
    for kk=2:1:(PP_length)
        P_comp_ideal(kk) = P_comp_ideal(kk-1)*(VPP_combined(
```

```
            kk-1)/...
                VPP_combined(kk))^gamma;
            if P_comp_ideal(kk) > P_dis_bulk
                P_comp_ideal(kk) = P_dis_bulk;
            end
        end
        BWcomp_ideal = -trapz(VPP_combined(1:end),(P_comp_ideal(1:end)*...
            (un.psi/un.Pa)));
else
end

if debug
    figure('name','Ideal Compression Plot')
    plot(VPP_combined*(un.m3/un.cc),P_comp_ideal*(un.psi/un.bar),'r--')
    hold on
    yline(P_dis_bulk*(un.psi/un.bar))
    yline(P_suc_bulk*(un.psi/un.bar))
    hold off
end

%loss calculations
Loss_comp= BWcomp - BWcomp_ideal;
%flow loss relative to idea suction
Percent_loss_comp = (Loss_comp/BWcomp_ideal)*100;
%Total Ideal BW
Total_ideal_BW = BW_ideal - BWsuc_ideal + BWcomp_ideal-BWsuc_start;
Total_ind_BW =BWd + BWcomp_singleline - Bwsuc_singleline - BWsuc_start;
%Percent Loss relative to ideal total ideal BW
Percent_loss_dis = (Loss_dis/Total_ideal_BW)*100;
Percent_loss_dis_pmc = (Loss_dis_pmc/Total_ideal_BW)*100;
Percent_loss_dis_valves = (Loss_valves/Total_ideal_BW)*100;
Percent_loss_dis_vp = (Loss_vp/Total_ideal_BW)*100;
Percent_loss_dis_plenum =(Loss_plenum/Total_ideal_BW)*100;
Percent_loss_suc = (Loss_suc/Total_ideal_BW)*100;

toc
```

APPENDIX B: Matlab Graphical User Interface

A Graphical User interface was developed using MATLAB (2020) for the purpose of allowing others to calculate the losses for the desired number of test conditions. The GUI then allowed for the losses to the displayed to a table and saved in a user defined location. The GUI additionally allows for the user to filter through test conditions based on specific user selected SST and SDT values. All of the conditions and losses then populate in list box that allow the user to select and plot any desired condition or loss.

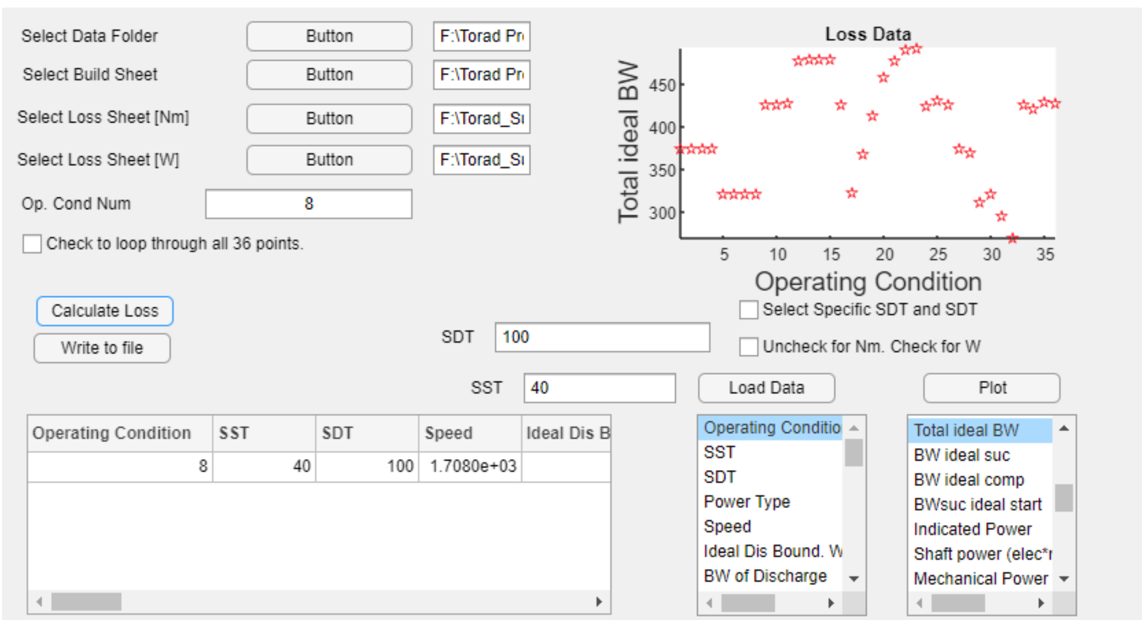

Figure B.1: All 20 pressures of each sensor overlaid showing off triggered samples.

APPENDIX C: Indicated Loss Analysis Data

The following tables consist of the relevant loss conditions and calculation as well as the relevant bulk data from the test stand.

Table C.1: Loss Data

Test #	SST	SDT	Speed	Ideal Dis BW	BW of Discharge
	C	C	rpm	N-m	N-m
1	4.44	43.33	1698.11	336.01	388.38
2	4.44	43.33	1470.77	336.32	383.30
3	4.44	43.33	1262.15	338.35	382.37
4	4.44	43.33	1060.30	321.14	358.77
5	4.44	37.78	1073.15	314.00	352.86
6	4.44	37.78	1276.98	334.82	380.87
7	4.44	37.78	1481.96	333.03	381.92
8	4.44	37.78	1708.04	325.78	383.79
9	4.44	48.89	1458.82	335.66	377.58
10	4.44	48.89	1250.68	337.97	376.51
11	4.44	48.89	1044.70	327.04	361.02
12	4.44	54.44	1026.10	338.96	371.50
13	4.44	54.44	1232.89	351.67	388.04
14	4.44	54.44	1442.44	348.87	385.19
15	4.44	54.44	1647.35	358.08	399.56
16	4.44	48.89	1663.53	343.20	390.41
17	-1.11	37.78	1757.21	280.89	309.96
18	-1.11	43.33	1750.57	275.77	311.43
19	-1.11	48.89	1742.26	297.18	327.83
20	-1.11	54.44	1735.99	298.02	331.90
21	4.44	54.44	1733.86	347.98	389.52
22	10.00	54.44	1731.03	398.13	452.59
23	15.56	54.44	1729.71	463.69	529.09
24	15.56	48.89	1739.41	460.96	533.27
25	10.00	48.89	1740.13	390.48	449.34
26	4.44	48.89	1740.90	335.85	385.81
27	4.44	43.33	1747.51	330.58	381.69
28	10.00	43.33	1747.38	389.47	453.35
29	10.00	37.78	1756.22	385.36	450.90
30	4.44	37.78	1756.35	323.28	377.13
31	4.44	35.00	1695.42	327.60	381.27
32	4.44	32.22	1698.83	331.31	391.92

Table C.1 continued from previous page

33	4.44	48.89	1664.30	336.63	369.04
34	1.67	48.89	1665.58	319.57	334.69
35	7.22	48.89	1662.84	364.86	391.66
36	12.78	48.89	1661.26	425.37	467.35

Table C.2: Loss Data Continued

Test #	Plenum BW	BW MC	BW Comp	BW Suc	Total Ind BW
	N-m	N-m	N-m	N-m	N-m
1	356.08	343.78	319.70	251.13	432.83
2	354.81	344.63	321.71	251.51	429.46
3	359.80	346.64	325.93	251.94	432.33
4	340.01	330.43	329.58	253.64	410.65
5	330.73	322.88	285.29	250.19	363.90
6	354.83	343.69	272.74	249.90	379.62
7	349.81	341.63	273.31	250.67	380.58
8	344.72	334.38	278.01	250.48	387.25
9	352.30	341.72	373.75	252.33	474.94
10	356.53	344.35	375.75	251.98	476.30
11	344.30	334.41	377.05	252.17	461.90
12	357.09	346.00	422.61	253.49	516.55
13	370.17	357.27	420.41	252.71	531.69
14	365.98	354.59	413.42	252.84	521.72
15	376.01	363.00	410.30	251.76	533.97
16	362.06	350.26	372.72	252.93	486.05
17	291.87	283.13	272.15	204.99	357.49
18	284.23	275.23	314.95	202.49	404.13
19	311.44	300.63	347.12	206.63	448.62
20	313.03	301.04	396.62	208.30	500.48
21	366.51	352.29	411.57	251.04	526.07
22	419.94	401.57	429.36	300.98	551.99
23	491.56	469.73	430.69	360.20	564.72
24	489.37	468.21	367.46	359.73	506.08
25	413.14	395.46	375.27	300.25	495.21
26	353.85	338.83	370.07	249.02	482.71
27	348.16	336.27	321.68	249.21	430.09
28	412.85	398.61	317.43	300.58	441.10
29	407.86	394.71	261.28	294.73	388.87
30	340.05	329.62	277.54	248.21	382.39
31	342.44	334.15	250.25	248.16	359.35
32	350.71	342.47	224.46	250.36	342.03
33	343.81	339.84	373.00	251.74	466.25
34	326.17	322.54	358.72	228.39	443.15

Table C.2 continued from previous page

35	374.36	370.29	374.01	276.41	462.72
36	437.83	432.57	376.68	331.60	480.57

Table C.3: Loss Data Continued

Test #	Total ideal BW	BW ideal suc	BW ideal comp	BWsuc ideal start
	N-m	N-m	N-m	N-m
1	374.43	256.35	318.91	24.13
2	374.32	256.43	318.48	24.04
3	374.38	256.43	316.49	24.03
4	374.11	256.40	333.42	24.06
5	321.51	256.43	288.00	24.05
6	321.37	256.38	267.02	24.09
7	321.47	256.48	268.89	23.98
8	321.43	256.37	276.10	24.08
9	426.56	256.44	371.40	24.06
10	426.65	256.54	369.19	23.98
11	427.20	256.48	380.64	24.00
12	478.43	256.46	419.99	24.06
13	479.04	256.43	407.86	24.05
14	479.24	256.57	410.99	24.05
15	479.21	256.44	401.70	24.13
16	426.61	256.40	363.96	24.15
17	322.87	209.83	271.44	19.63
18	368.41	210.33	322.72	19.75
19	413.23	209.59	345.34	19.70
20	458.43	210.20	390.34	19.73
21	478.53	256.53	411.06	23.98
22	490.85	310.03	431.73	28.98
23	493.21	371.71	436.09	34.86
24	424.32	371.49	369.77	34.92
25	430.94	309.77	379.39	29.16
26	426.55	256.30	371.15	24.16
27	374.25	256.44	324.19	24.07
28	370.31	310.01	319.95	29.10
29	311.18	304.51	258.92	28.58
30	321.72	256.40	278.91	24.07
31	295.47	255.25	247.15	24.02
32	269.19	255.83	217.69	23.99
33	426.61	256.45	370.50	24.07
34	421.47	232.38	356.15	21.86
35	429.96	282.16	373.79	26.54
36	428.70	339.78	374.97	31.86

Table C.4: Loss Data Continued

Test #	Discharge Loss	Plenum Loss	MC Loss	Valve Loss	Suc Loss
	N-m	N-m	N-m	N-m	N-m
1	52.38	12.30	7.78	32.30	5.10
2	46.97	10.18	8.31	28.49	4.92
3	44.02	13.16	8.29	22.57	4.44
4	37.63	9.58	9.29	18.76	2.65
5	38.86	7.85	8.88	22.13	6.21
6	46.05	11.15	8.87	26.04	6.42
7	48.89	8.17	8.60	32.12	5.55
8	58.01	10.34	8.60	39.07	5.73
9	41.92	10.57	6.06	25.28	4.00
10	38.54	12.18	6.38	19.98	4.38
11	33.98	9.89	7.38	16.72	4.19
12	32.54	11.09	7.04	14.41	2.83
13	36.38	12.89	5.61	17.87	3.65
14	36.32	11.39	5.72	19.21	3.69
15	41.47	13.01	4.92	23.55	4.64
16	47.21	11.80	7.06	28.34	3.27
17	29.06	8.74	2.23	18.09	4.66
18	35.66	9.00	-0.55	27.20	7.77
19	30.65	10.80	3.45	16.40	2.84
20	33.88	11.99	3.03	18.86	1.87
21	41.54	14.22	4.31	23.01	5.38
22	54.46	18.37	3.45	32.65	8.84
23	65.40	21.83	6.04	37.53	10.98
24	72.31	21.16	7.25	43.90	11.74
25	58.86	17.68	4.98	36.20	9.52
26	49.96	15.02	2.98	31.96	7.07
27	51.12	11.88	5.70	33.53	7.24
28	63.88	14.23	9.14	40.50	9.43
29	65.54	13.15	9.35	43.04	9.61
30	53.85	10.43	6.34	37.08	8.07
31	53.67	8.29	6.55	38.83	6.97
32	60.61	8.24	11.16	41.21	5.19
33	32.42	3.97	3.22	25.24	4.69
34	15.11	3.63	2.97	8.52	4.00
35	26.79	4.07	5.43	17.30	5.81
36	41.97	5.26	7.20	29.52	8.17

Table C.5: Loss Data Continued

Test #	Comp Loss	Valve Loss	Plenum Loss	MC Loss	Loss Comp
	N-m	%	%	%	%
1	0.97	8.63	3.28	2.08	0.26
2	3.33	7.61	2.72	2.22	0.89
3	9.50	6.03	3.51	2.22	2.54
4	-3.69	5.02	2.56	2.48	-0.99
5	-2.66	6.88	2.44	2.76	-0.83
6	5.94	8.10	3.47	2.76	1.85
7	4.92	9.99	2.54	2.67	1.53
8	2.20	12.16	3.22	2.67	0.68
9	2.59	5.93	2.48	1.42	0.61
10	6.96	4.68	2.86	1.49	1.63
11	-3.26	3.91	2.32	1.73	-0.76
12	2.78	3.01	2.32	1.47	0.58
13	12.87	3.73	2.69	1.17	2.69
14	2.51	4.01	2.38	1.19	0.52
15	8.72	4.91	2.71	1.03	1.82
16	9.14	6.64	2.77	1.65	2.14
17	1.18	5.60	2.71	0.69	0.36
18	-7.58	7.38	2.44	-0.15	-2.06
19	2.13	3.97	2.61	0.84	0.52
20	6.44	4.12	2.62	0.66	1.41
21	1.00	4.81	2.97	0.90	0.21
22	-1.75	6.65	3.74	0.70	-0.36
23	-4.64	7.61	4.43	1.23	-0.94
24	-1.74	10.34	4.99	1.71	-0.41
25	-3.98	8.40	4.10	1.15	-0.92
26	-0.65	7.49	3.52	0.70	-0.15
27	-2.35	8.96	3.18	1.52	-0.63
28	-2.39	10.94	3.84	2.47	-0.65
29	2.55	13.83	4.23	3.01	0.82
30	-1.16	11.53	3.24	1.97	-0.36
31	3.32	13.14	2.80	2.22	1.12
32	7.24	15.31	3.06	4.14	2.69
33	2.64	5.92	0.93	0.75	0.62
34	2.65	2.02	0.86	0.70	0.63
35	0.28	4.02	0.95	1.26	0.07
36	2.36	6.89	1.23	1.68	0.55

Table C.6: Loss Data Continued

Test #	Loss Discharge	Total Ind Loss	Total BW Uncertainty
	%	N-m	%
1	13.99	58.45	0.852247
2	12.55	55.22	0.858547
3	11.76	57.96	0.858741
4	10.06	36.59	0.869748
5	12.09	42.41	0.862762
6	14.33	58.41	0.843053
7	15.21	59.35	0.845159
8	18.05	65.94	0.845834
9	9.83	48.51	0.898766
10	9.03	49.88	0.88149
11	7.95	34.90	0.945002
12	6.80	38.14	1.353722
13	7.59	52.89	1.245051
14	7.58	42.52	1.090742
15	8.65	54.84	1.260101
16	11.07	59.61	1.099021
17	9.00	34.90	0.938101
18	9.68	35.85	0.879228
19	7.42	35.62	0.93803
20	7.39	42.19	1.093039
21	8.68	47.93	1.132166
22	11.10	61.55	1.21243
23	13.26	71.74	1.131639
24	17.04	82.31	0.929074
25	13.66	64.40	0.844187
26	11.71	56.39	0.898308
27	13.66	56.00	0.859809
28	17.25	70.92	0.86037
29	21.06	77.70	0.860539
30	16.74	60.76	0.864398
31	18.17	63.97	0.846696
32	22.51	73.04	0.875121
33	7.60	39.75	0.947115
34	3.59	21.76	1.003298
35	6.23	32.88	0.978193
36	9.79	52.50	0.915569

Table C.7: Relevant Bulk Load Stand Data

Test #	Bulk Suc Pressure	Bulk Suc Temp	Bulk Dis Temp	Electric Power
	bar	C	C	kW
1	3.43	15.57	69.23	27.53
2	3.43	15.54	69.56	23.84
3	3.43	15.58	70.70	20.90
4	3.43	15.57	72.50	16.72
5	3.43	15.53	64.83	14.79
6	3.43	15.54	63.11	18.28
7	3.43	15.55	62.33	21.07
8	3.43	15.54	62.44	24.56
9	3.43	15.61	76.72	26.32
10	3.43	15.53	77.97	23.05
11	3.43	15.57	80.73	18.91
12	3.43	15.53	90.25	21.45
13	3.43	15.60	88.14	25.98
14	3.43	15.57	84.25	29.27
15	3.43	15.59	83.82	33.72
16	3.43	15.58	76.01	30.25
17	2.81	10.01	64.68	24.22
18	2.82	10.03	70.41	26.57
19	2.81	10.02	77.88	29.27
20	2.81	10.00	85.84	32.34
21	3.43	15.55	81.50	33.90
22	4.15	21.13	78.17	35.13
23	4.98	26.60	75.97	35.92
24	4.97	26.62	69.85	32.03
25	4.15	21.11	71.25	31.50
26	3.43	15.56	73.64	30.80
27	3.43	15.59	68.00	27.65
28	4.15	21.07	65.77	28.12
29	4.08	21.00	60.68	25.07
30	3.43	15.72	61.89	24.81
31	3.42	15.62	59.43	22.60
32	3.42	15.60	56.81	21.38
33	3.43	15.52	75.32	30.13
34	3.11	12.75	76.48	29.53
35	3.78	17.97	73.76	30.55
36	4.55	23.90	71.91	31.46

APPENDIX D: Supplemental Experimental Testing

To continue progression in the initiate to improve the spool compressor performance additional supplemental testing was performed on a 40 ton displacement spool compressor using R134a and R1234ze. A hot-gas bypass compressor test load stand was designed and developed by Schmidt et al. (2019) to test low GWP refrigerants on compressors. The same compressor test load stand was commissioned for independent testing by Singleton (2020). That developed hot gas bypass compressor load stand was used as the test environment in this testing and will be referred to the OSU load stand. Modifications needed to be made on the OSU load stand to allow for testing of the 40 ton open drive spool compressor such new manifold construction, oil line modification to allow for oil to be directly pumped into the compressor and the installation of a torque cell needed to measure shaft torque. Table D.1 shows the test conditions that were selected to be run on both refrigerants in order to capture a wide range of conditions that can give be of added value when working to improve the spool compressor comprehensive model presented in Bradshaw and Groll (2013). Both R134a and R1234ze were tested using the test matrix shown in Table D.1. The OSU load stand collected the bulk steady-state temperatures, pressures, mass flow rates, and efficiencies as data compliant with ASHRAE-23.1 (2010) compressor testing standards. Results from this testing may be published in future publication.

Table D.1: Test Matrix for 40 Ton open drive spool compressor supplemental testing.

Pts	**Speed**	**SST**	**SDT**	**DTsuc**
	RPM	C	C	R
1	1650	4.44	43.33	20
2	1650	4.44	46.11	20
3	1650	4.44	48.89	20
4	1650	4.44	54.44	20
5	1650	4.44	51.67	20
6	1650	5.56	51.67	20
7	1650	10.00	51.67	20
8	1650	-1.11	51.67	45
9	1650	-6.67	51.67	60
10	1750	4.44	51.67	20
11	1800	4.44	51.67	20
12	1550	4.44	51.67	20
13	1650	5.56	23.89	20
14	1650	5.56	26.67	20
15	1650	5.56	32.22	20
16	1650	5.56	37.78	20

Table D.1 continued from previous page

17	1650	5.56	43.33	20
18	1650	5.56	48.89	20
19	1650	5.56	54.44	20
20	1650	5.56	60.00	20
21	1050	5.56	37.78	20
22	1200	5.56	37.78	20
23	1350	5.56	37.78	20
24	1500	5.56	37.78	20
25	1650	5.56	37.78	20
26	1800	5.56	37.78	20
27	1650	10.00	37.78	20
28	1650	4.44	37.78	20
29	1650	-1.11	37.78	20
30	1650	-6.67	37.78	20
31	1650	-12.22	37.78	20
32	1650	-17.78	37.78	20
33	1650	-23.33	37.78	20
34	1650	5.56	37.78	15
35	1650	5.56	37.78	**20**
36	1650	5.56	37.78	25
37	1650	5.56	37.78	30
38	1650	5.56	37.78	35
39	1650	5.56	37.78	40
40	1650	5.56	37.78	45
41	1650	5.56	37.78	50
42	1650	-23.33	23.89	20
43	1650	-23.33	54.44	20
44	1650	10.00	23.89	20
45	1650	10.00	54.44	20
46	1650	10.00	37.78	Fixed Suction Temp at 18.33 C
47	1650	4.44	37.78	
48	1650	-1.11	37.78	
49	1650	-6.67	37.78	
50	1650	-12.22	37.78	
51	1650	-15.00	37.78	
52	1650	-23.33	37.78	
53	1650	10.00	23.89	20
54	1650	10.00	43.33	20
55	1650	10.00	54.44	20
56	1650	4.44	23.89	20
57	1650	1.67	23.89	20
58	1650	-1.11	23.89	20

VITA

Seth J Yarborough

Candidate for the Degree of

Master of Science

Thesis: EMPIRICAL INDICATED LOSS ANALYSIS OF A SEMI-HERMETIC LIGHT-COMMERCIAL SPOOL COMPRESSOR

Major Field: Mechanical and Aerospace Engineering

Biographical:

Education:

Completed the requirements for the Master of Science in Mechanical and Aerospace Engineering at Oklahoma State University, Stillwater, Oklahoma in May, 2021.

Completed the requirements for the Bachelor of Science in Mechanical Engineering at Oklahoma State University, Stillwater, Oklahoma in 2018.